Zinc and Nitrogen Co-doped TiO_2/ Graphene Oxide Nanocomposites for Photocatalytic Degradation of Methyl Orange

Name: Soha Safdar
Reg. # 00000117306

This thesis is submitted as a partial fulfillment of the requirements for the degree of
Master of Science in
Chemistry

Supervised by: Prof. Dr. Habib Nasir
Department of Chemistry
School of Natural Sciences (SNS)
National University of Sciences and Technology (NUST)
H-12, Islamabad, Pakistan

August, 2019

FORM TH-4

National University of Sciences & Technology

MS THESIS WORK

We hereby recommend that the dissertation prepared under our supervision by: Soha Safdar, Regn No. 00000117070 Titled: Zinc and Nitrogen Co-doped TiO2/ Graphene Oxide Nanocomposites for Photocatalytic Degradation of Methyl Orange be accepted in partial fulfillment of the requirements for the award of **MS** degree.

Examination Committee Members

1. Name: DR. MUHAMMAD ARFAN Signature:

2. Name: DR. MUDASSIR IQBAL Signature:

External Examiner: DR. ABDUL MATEEN Signature:

Supervisor's Name PROF. HABIB NASIR Signature:

Head of Department

05/09/2019
Date

COUNTERSINGED

Date: 05/9/2019

Dean/Principal

THESIS ACCEPTANCE CERTIFICATE

Certified that final copy of MS thesis written by **Ms. Soha Safdar,** (Registration No. **00000117070**), of **School of Natural Sciences** has been vetted by undersigned, found complete in all respects as per NUST statutes/regulations, is free of plagiarism, errors, and mistakes and is accepted as partial fulfillment for award of MS/M.Phil degree. It is further certified that necessary amendments as pointed out by GEC members and external examiner of the scholar have also been incorporated in the said thesis.

Signature: _____

Name of Supervisor: Prof. Habib Nasir

Date: 05/09/2019

Signature (HoD): _____

Date: 05/09/2019

Signature (Dean/Principal): _____

Date: 08/9/2019

In the name of ALLAH, the Gracious, the Merciful

Dedicated to

My family for their love, support and encouragement and my beloved daughter

Acknowledgements

*First of all, I would like to thank **Allah Almighty**, who has given me the ability, courage and His blessings to complete this thesis.*

*My special and sincere thanks to my supportive supervisor, **Prof. Dr. Habib Nasir** for providing me a peaceful environment to work and guiding me throughout my research work. A special thanks to my guidance and evaluation committee members, **Dr. Muhammad Arfan** and **Dr. Mudassir Iqbal**, for their valuable guidance, suggestions and encouragement. I am grateful especially to **School of Natural Sciences**, **NUST** for providing me all the facilities and a platform to work. I greatly acknowledge the facilities and technical support provided by other schools of NUST like **SMME, CASEN** and other institutes like **National Centre for Physics** and **Quaid-e-Azam University, Islamabad**.*

*Finally, I would like to express my gratitude to my righteous friends **Komal javed** & **Fareha Gul** for their loyal support, guidance, encouragement and prayers. I would like to thank my family members specially my parents and in-laws for their support, continuous encouragement and prayers, my husband **Muhammd Jahanzeb**, for always being there and helping me whenever needed throughout the research and writing process of this thesis. Without them, this achievement would not have been possible.*

Soha Safdar

Abstract

Textile industry contributes to 17 to 20% waste water pollution because of its intensive use of dyes. Dyes pose a significant threat to the environment due to their toxic nature. The most efficient method considered for the removal of these dyes is photocatalysis. Recent research on semiconductors has proven that TiO_2 is the best semiconductor so far for degradation of dyes. Having a large band gap of 3.2ev, fast electron hole recombination, TiO_2 absorbs only UV range of light. In this thesis, an effort to enhance its properties was done via codoping with a non-metal (Nitrogen) and a metal (Zinc) and then making a composite with graphene oxide (GO) nanosheets. TiO_2 nanoparticles were prepared using Sol-Gel method and varying concentrations of zinc (0.1%, 0.5%, 1%, and 2%) were used while keeping nitrogen concentration constant. Methyl orange (MO) is used to study the degradation activity in visible light. 2% Zn/N-codoped TiO_2 showed maximum activity of 80% in 24 hours. GO nanosheets were synthesized using Hummers method. Composites were formed using the best prepared catalyst and GO with varying ratios of GO (0.5:1, 1:1, 2:1) using Hydrothermal method. Further degradation studies were done using the prepared nanocomposites. The nanocomposites exhibited enhanced photocatalytic activity of 85% against MO in 10 hours. Various characterization techniques involving SEM, XRD, EDS, UV/Vis-spectroscopy were used to analyze the prepared nanoparticles & nanocomposites. Overall decrease in both grain size and crystallite size was observed.

Table of Contents

List of Figures

List of Tables

List of Abbreviations

CB	Conduction Band
DRS	Diffuse Reflectance Spectroscopy
EDX	Energy Dispersive X-Ray Spectroscopy
eV	Electron Volt
GO	Graphene Oxide
hr	Hour
MO	Methyl Orange
mg	Milligram
ml	Milliliter
min	Minute
SEM	Scanning Electron Microscopy
UV-Vis	Ultra Violet-Visible Spectroscopy
VB	Valence Band
XRD	X-Ray Diffraction

1 INTRODUCTION

1.1 Background

Water pollution has emerged as a great concern in recent years. Textile industry also contributes to it. The textile waste consist of dyes that pose threat to both waterbodies as well as human life [1].

Dyes are organic aromatic, ionizing compounds that are soluble in water. They are classified based on their origin as either natural or synthetic. Natural dyes are derived from animal or plant origin. Synthetic dyes can be categorized as azo and non-azo dyes [2].

Research is being done intensively in this field to remove these dyes from water [3]. The extraction and degradation of dyes is of significant concern because of their potential toxicity visibility in surface waters. A variety of techniques have been created, and heterogeneous photocatalysis containing titanium dioxide (TiO_2) is the best method [4].

1.2 Photocatalysis

Organic pollutants are partially or completely mineralized by semiconductor photocatalysis. Semiconductors bring about redox reaction, when irradiated with UV/Visible light in the audience of water and air [5].

1.2.1 Photocatalyst

ZnO and TiO_2 are the most effective photocatalysts among many other semiconductors used. But the main limitation of these semiconductors is the small value of quantum efficiency that causes fast electron hole recombination [6]. Nanosized TiO_2 is the best among the semiconductors because it has many interesting properties and a tunable band gap of 3.2ev making it useful for dye degradation [7,8].

1.2.2 Degradation Mechanism

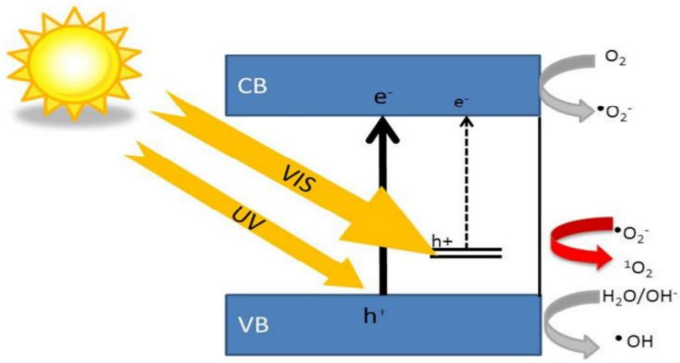

Figure 1.1 Photocatalysis mechanism

Semiconductor is irradiated with a photon of light causing excitation of e^- of the valence band (VB) towards the conduction band (CB) of the semiconductor. This excited e^- leaves h^+ behind within the valence band. The excited e^- within the CB carries out reduction process while oxidation is carried out by the h^+ in the VB [9].

Despite being said to be the most promising semiconductor, TiO_2 has a huge bandgap of 3.2ev with fast e^-/h^+ recombination reducing its photocatalytic degradation activity. So it has room for improvement in the structure and bulk properties which can be done using a variety of techniques. **Figure 1.2** shows an extensive range of techniques that can be applied to boost the properties of TiO_2 [10].

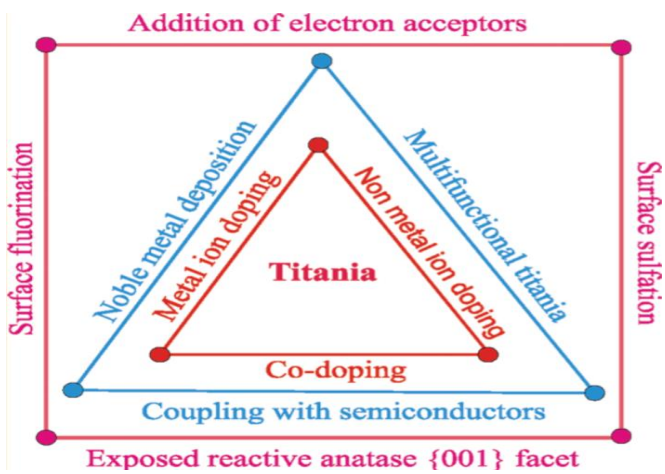

Figure 1.2 Techniques for structural modification in TiO_2

The best and effective method for the improvement of photocatalytic activity of TiO_2 is doping. Doping enhances the photocatalytic activity by causing reduction in the band gap of TiO_2, also restricting the e^-/h^+ recombination. The decrease in the band gap makes possible the immersion of visible portion of light. TiO_2 can be doped by either a metal, a non-metal or it can be co-doped with both of them [11].

1.3 Co-doping in TiO_2

Efforts to enhance the properties of TiO_2 for practical applications has been done in the past by doping with transition and noble metal ions[12].TiO_2 can be doped using Cr, Cu, Fe, Mn, Zn, V, Ag and W etc.[13]. Zn dopants can increase surface defects and reduce the e^-/h^+ recombination in TiO_2 [14].

Sato et al. noted that NOx species can significantly narrow the TiO_2 band gap, which extends its spectrum of absorption within the region of visible light. Their study gave rise to an increasing interest in TiO_2 non-metal doping [15]. Nitrogen doped TiO_2 shows increased photocatalytic activities among many other non-metals by causing narrowing of bandgap in TiO_2 and blocking reoxidation [16].

Recently, researcher have been trying to co-dope TiO_2 with both metal and non-metals. The addition of two dopant species causes decrease in crystallite and particle size, reduced bandgap, increased surface area, increased absorption capability and an effective decrease in e^-/h^+ recombination resulting in enhanced photocatalytic activity. All these properties are enhanced because of the added effect of both metal and non-metal addition [17].

1.4 TiO_2/ Graphene oxide (GO) nanocomposites

The composite of GO and TiO_2 has the characteristics of both a single layered material with greater surface area and a metal oxide that makes it easy to generate electrons and holes [18]. Potentially enhanced photocatalytic activity is presented by TiO_2/ GO nanocomposites because of the amplified surface area, excellent adsorption and decreased e^-/h^+ recombination at the interface [19].

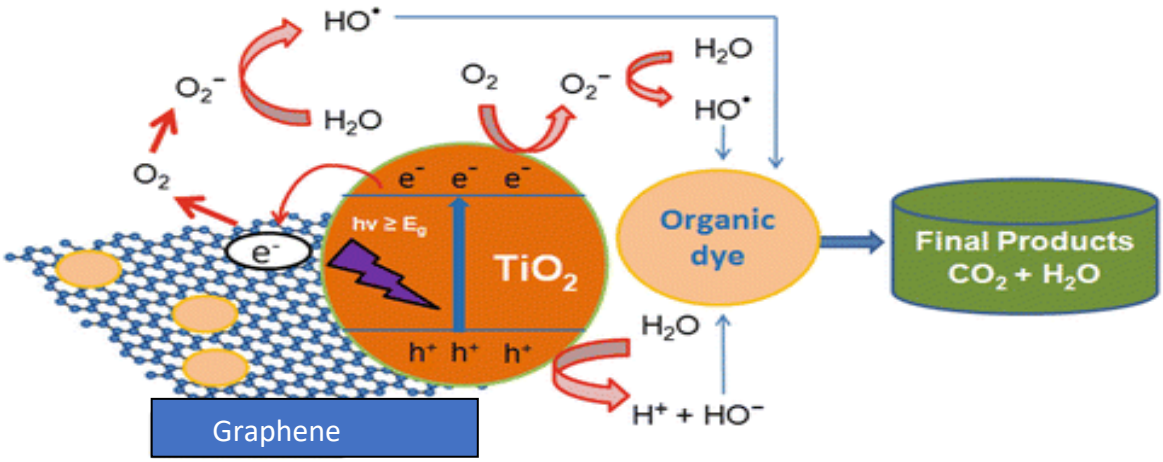

Figure 1.3 Photocatalytic activity of TiO_2/ GO nanocomposites under UV-visible light

1.5 Synthesis of TiO_2 nanoparticles

Many efforts have been made in order to manufacture based on a variety of methods. TiO_2 has various morphologies including mesoporous structures, nanorods, nanotubes, nanowires and nanoparticles having different properties attributing to their varying structures. These morphologies depend upon the method of synthesis used. Following are some of the methods used for the synthesis of TiO_2 [20]:

a) Hydrothermal method

b) Solvothermal method

c) Sol-gel method

d) Direct oxidation method

e) Chemical vapor deposition

f) Electrodeposition

g) Sonochemical method

h) Microwave method

1.5.1 Sol-gel method

Sol-gel method is a flexible technique used to manufacture advanced materials, such as organic-inorganic hybrids etc. This technique has been improved in recent years with commercialization and development and it is now one of the most efficient synthesis technique in nanotechnology. The benefits of using this technique involve

stoichiometric control of precursor solutions, easy alteration in composition, easy introduction of different functional groups and inexpensive process [21].

Figure 1.4 Shows sol-gel synthesis of TiO_2 nanoparticle [22].

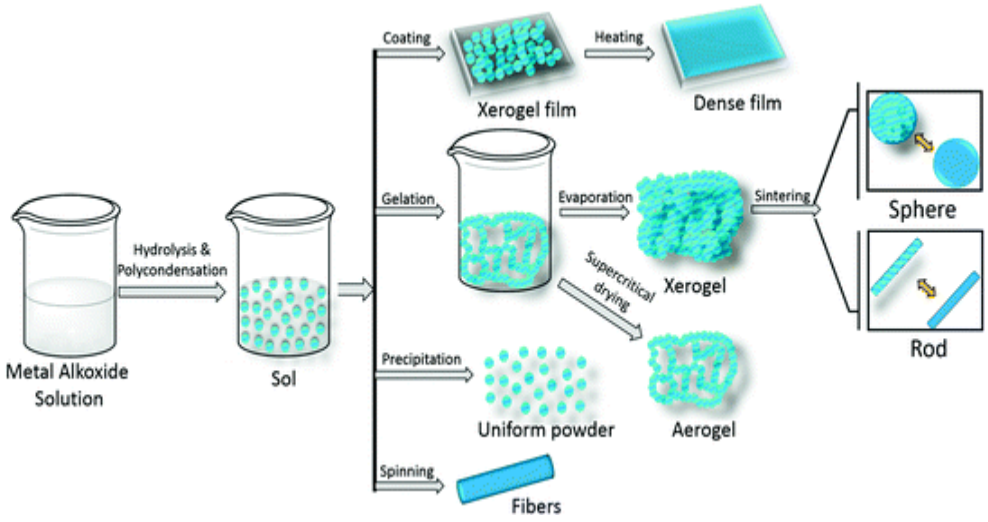

Figure 1.4 Sol-gel synthesis of TiO_2 nanoparticles

Following steps are involved in sol-gel method [23]:

1. Mixing
2. Casting
3. Gelation
4. Aging
5. Drying
6. Densification

1.6 Synthesis of graphene oxide nanosheets

Following are the three basic techniques used for synthesis of graphene oxide or some variation of these methods:

a) Brodie
b) Staudenmaier
c) Hummers'

The first two procedures use potassium chlorate ($KClO_3$) with nitric acid (HNO_3) causing oxidation of Graphite while hummers' method uses sulfuric acid (H_2SO_4) and potassium permanganate ($KMnO_4$). **Figure 1.5** shows framework of graphene oxide [24].

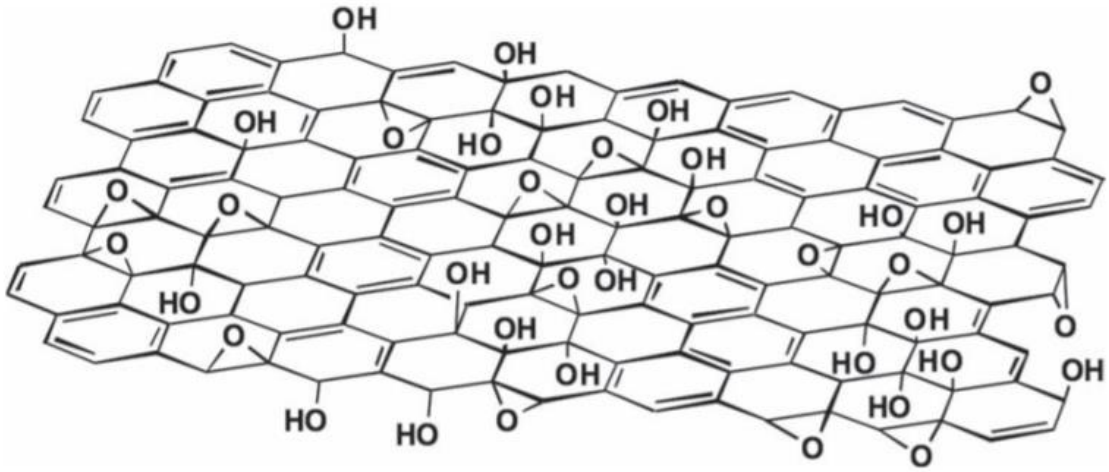

Figure 1.5 Structural diagram of graphene oxide

1.6.1 Hummers' method

It is the most frequently used method for graphene oxide synthesis because it's fast, inexpensive and simple method.

Graphite powder is taken and H_2SO_4 to it while maintaining the temperature at 0-5°C. $NaNO_3$ is added to this mixture and left for continuous stirring for 2 hours. The temperature is then maintained at 15 °C while adding $KMnO_4$ to the solution slowly. After that, the temperature is maintained to 35°C with continuous stirring for 2 days. Grey colored slurry is formed. Water is added slowly changing the color of the solution to brown. H_2O_2 is added slowly to terminate the reaction which further changes the brown colored solution to yellow. The obtained solution is allowed to settle down. It is then decanted, sonicated and washed with HCl and H_2O numerous times. It is dried out in oven for 24 hours and GO is obtained [25].

1.7 Synthesis of TiO_2/ GO nanocomposites

TiO_2/ GO nanocomposites can be synthesized using a variety of techniques:

1. Microwave heating

2. In-Situ chemical synthesis
3. Hydrothermal and solvothermal method

1.7.1 Hydrothermal and solvothermal method

It is a well-known technique that uses elevated temperature and pressure for nanostructures synthesis. The method is performed in a closed system and the solvent used is mostly water, so this method is deemed environmentally friendly. Depending on the potential of the autoclave container, highly pure crystals can be created in bulk. This method is broadly described for the production of graphene/inorganic nanostructures composites: CuO/graphene [26], ZnO/graphene [27] and SnO_2/graphene [28].

Solvents, such as ethanol, methanol etc. can also be used. This process is identified as solvothermal method when water is used as a solvent.

1.8 Dyes

Dye is a kind of pigment used to color various substances, but mostly used on products made of fibers and leather. Dyes are organic compounds that are aromatic and have affinity to specific substances. Most of them are used as aqueous solutions. Auxochromes i.e.-OH,-Cl,-Br,-NO_2,-COOH,-NHR,-NH_2 etc. are the reason for solubility of dyes in water as they ionize in water. They intensify the color of dyes as well. Auxochromes can be categorized as acidic or basic, depending on their charge and nature [29].

1.8.1 Types of dyes

Mainly dyes are classified as:

a) Natural dyes
b) Synthetic dyes

Natural dyes are extracted from animals and plants origin. Natural dyes obtained from sea snails and madder root are Tyrian purple and madder respectively. Synthetic coloring is categorized as non-azo coloring and azo coloring. Furthermore, azo colors are categorized as acidic, basic and reactive, dispersed and Sulfur dyes. Synthetic colors,

depending on their nature, can also be categorized as basic and acidic. **Figure 1.6** shows the flow chart for the classification of dyes.

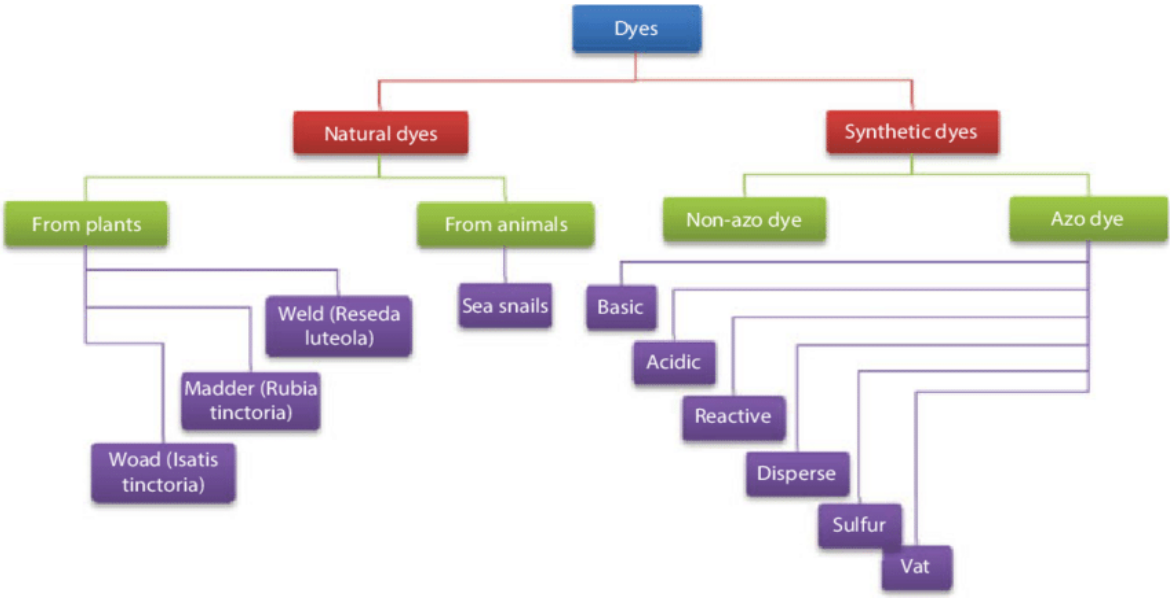

Figure 1.6 Flow chart for classification of dyes

1.8.2 Disadvantages of dyes

Although dyes have many advantages, in many distinct respects they are also hazardous to human life. Following are the various risks posed by dyes [30]:

- Dyes are mostly water-soluble and therefore cause water pollution. When discharged into waterways, this water causes serious harm to both aquatic and human lives.
- Dyeing affects the absorption and reflection of sunlight from water and therefore affects the photosynthetic activity underwater.
- Many dyes are cancerous and some may trigger skin irritation.
- The transparency of the water bodies is significantly influenced by the narrow amount of dyes that cannot even be detected by the human eye.

For the survival of living organisms, these damaging colors must be removed or better degraded.

1.8.3 Methyl orange

It is an orange dye which is commonly used as a pH indicator. Its color changes from orange to yellow in basic environment.

Methyl orange's molecular structure is altered when the solution's pH is altered, signaled by the change in methyl orange color. Hydrogen ion is connected to the N= N bond nitrogen atom under acidic circumstances and thus changes the molecular structure [31].

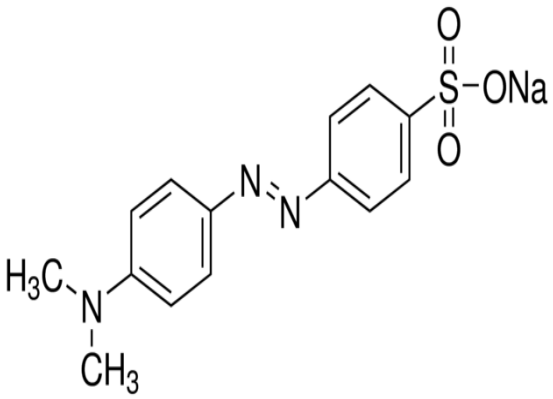

Figure 1.7 Structure of methyl orange

1.8.4 Mechanism of dye degradation

In **figure 1.8**, it is seen that after the irradiation of photocatalyst, production of e^-/h^+ pair occurs and the dye is degraded. Dye degradation occurs by the CB's electrons of the semiconductor.

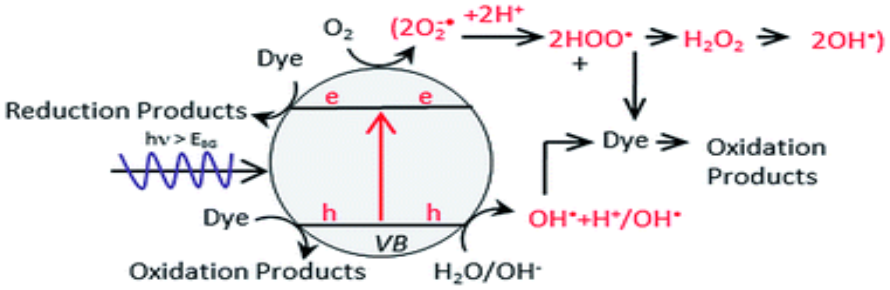

Figure 1.8 Dye degradation under light irradiation

The valence band (VB) holes play an essential role in inducing a photocatalytic oxidation reaction to decompose environmental pollutants. The holes in the valence

band react with water and produceA hydroxyl radicals ($OH^{\bullet}$) instead of directly oxidizing pollutants [32].

The basic mechanism of pollutant degradation is shown in the following equations from (i) to (viii):

$$TiO_2 + h\nu \longrightarrow TiO_2\,(e^-_{CB} + h^+_{VB}) \quad \text{(i)}$$

$$TiO_2\,(h^+_{VB}) + H_2O \longrightarrow TiO_2 + H^+ + OH^{\bullet} \quad \text{(ii)}$$

$$TiO_2\,(h^+_{VB}) + OH^- \longrightarrow TiO_2 + OH^{\bullet} \quad \text{(iii)}$$

$$TiO_2\,(e^-_{CB}) + O_2 \longrightarrow TiO_2 + O_2^{\bullet -} \quad \text{(iv)}$$

$$O_2^{\bullet -} + H^+ \longrightarrow HO_2^{\bullet} \quad \text{(v)}$$

$$\text{Dye} + OH^{\bullet} \longrightarrow \text{Degradation products} \quad \text{(vi)}$$

$$\text{Dye} + h^+_{VB} \longrightarrow \text{Oxidation products} \quad \text{(vii)}$$

$$\text{Dye} + e^-_{CB} \longrightarrow \text{Reduction products} \quad \text{(viii)}$$

1.9 Characterization techniques

After nanomaterials synthesis, analysis of purity of the phase, particle size, crystallite size, surface morphology, elemental composition and optical properties is done. A variety of techniques are used including powder X-ray diffractometry, Scanning Electron Microscopy, Thermogravimetry, UV-Visible Spectroscopy and Electron Spin Resonance Spectroscopy. They will be shortly discussed in the chapter below.

1.9.1 Scanning electron microscopy (SEM)

Its basic functioning depends on the thermionically emitted electrons from a tungsten source and that move towards an anode as can be seen in **figure 1.9**. The entire system is kept under a very heavy vacuum. One or two condenser lenses with an extremely good focal spot size (1 nm to 5 nm) focus the electron beam with an energy (-50 keV). The SEM pictures are of three kinds including: (i) Secondary electron pictures (ii) Back-scattered electron pictures and (iii) Elemental X-ray maps. If their energy is less than 50 eV, the electrons are referred to as secondary electrons. The secondary electrons are emitted from the few nm of the surface and thus provide the surface data.

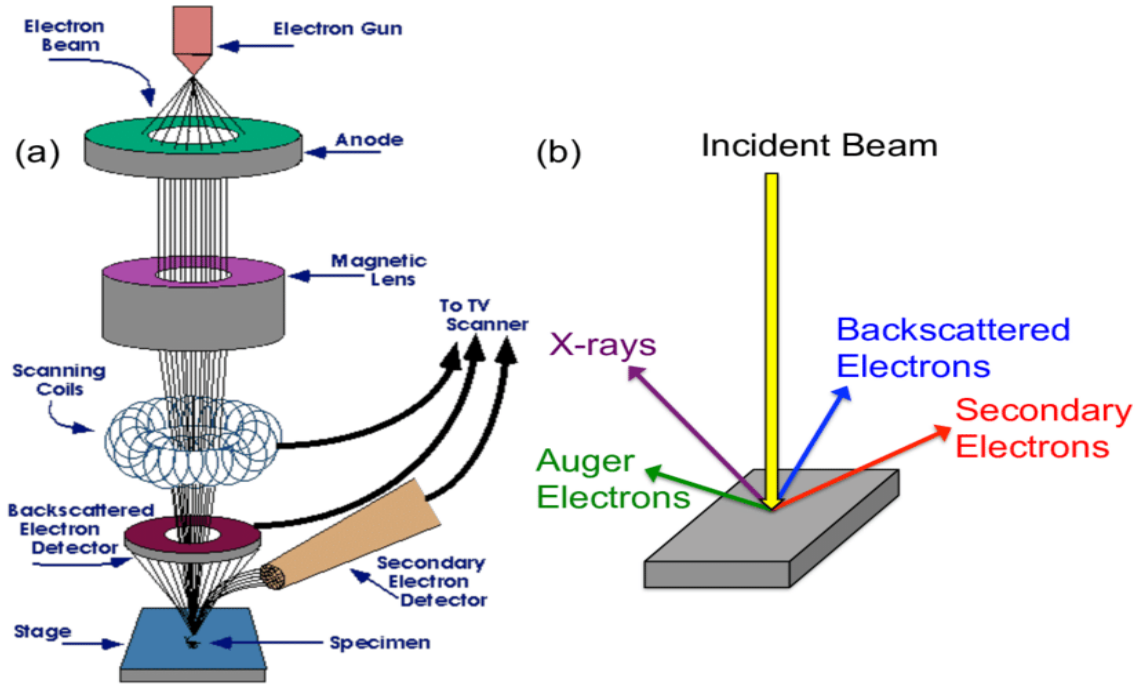

Figure 1.9 Schematic illustration of SEM

1.9.2 Energy dispersive X-ray spectroscopy (EDS or EDX)

When an incident beam is allowed to drop on a sample, it produces a hole in the shell after ejection of an excited electron from an internal shell. As a result, an electron from an external shell falls into the inner shell to fill that vacancy. The power distinction among the higher shell and the lower shell is caused by X-ray emissions.

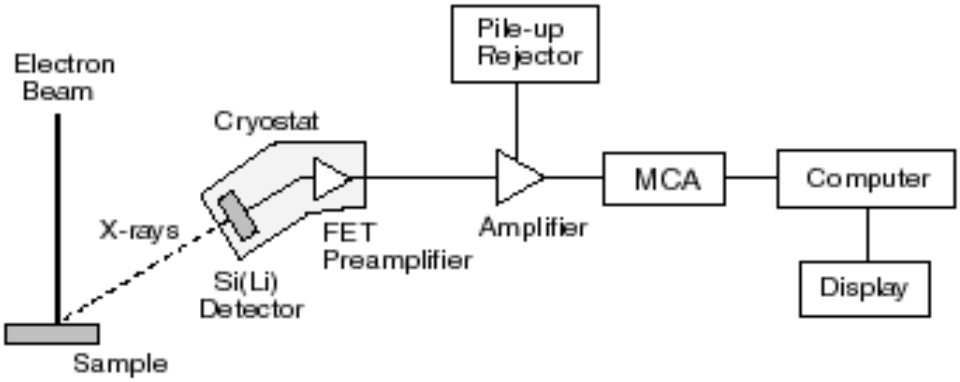

Figure 1.10 Schematic illustration of EDS/EDX

An energy dispersive spectrometer is used to determine the amount and energy of the X-ray released from a sample. The elemental configuration of the sample can be determined as the energy of the X-rays is specific to every element. **Figure 1.10** illustrates the basic scheme of EDX machine.

1.9.3 X-ray diffraction (XRD)

In this technique, at an angle θ to the atomic planes, an X-ray beam of a particular wavelength (π) is focused on the crystal. These X-rays interact with the atoms ' electrons and the atomic planes return them back. Since the crystal structure's atomic planes are deemed semi-transparent, they enable a share of the X-rays to permit through and return the other portion. The reflected angle is equivalent to the incident angle θ as shown in **figure 1.11**; it is also called Bragg angle.

Bragg's law: $\mathbf{2d\sin\theta = n\lambda}$

The unit size of crystallites can be determined by applying Scherrer's formula.

Scherer's formula: $\mathbf{D = K\,\lambda / B\cos\theta}$

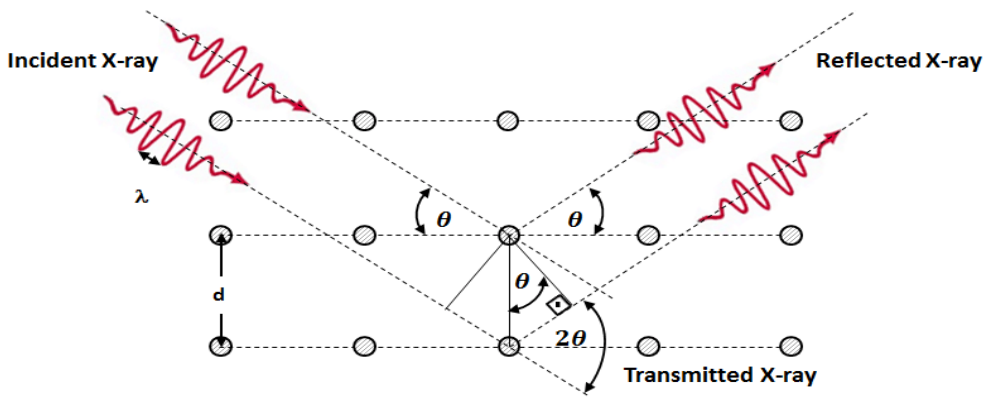

Figure 1.11 Bragg's law of diffraction

The distinctive X-rays generated by an X-ray are collimated and focused onto the specimen. The specimen and detector are subsequently revolved to record the amount of the X-rays reflected, which a detector processes further. Detector's role is to transform the signal and then send it to a computer monitor. There is a tool known as a goniometer inside the XRD machine that is used to retain the angle and rotate the specimen. Filters of Zn and Ni are used to prevent undesirable radiation.

1.9.4 UV-visible absorption spectroscopy

A distinctive sample absorption spectrum is acquired by evaluating the sample's absorption in relation to the light frequency. The distinctive lines found in the isolated atom absorption spectrum are very sharp, which helps to correctly determine the photon wavelength.

For its identification, these streaks are distinctive of a specific atom or ion. As age degeneration occurs in solids at atomic levels, it provides wide optical spectrum. The energy difference between the highest occupied molecular orbital (HOMO) and the lowest unoccupied molecular orbital (LUMO) bands is designated as the fundamental gap. Since UV / Vis spectroscopy's penetration depth is only 50 nm, it cannot be used for bulk solids, however, this method is extremely important to nanomaterial characterization.

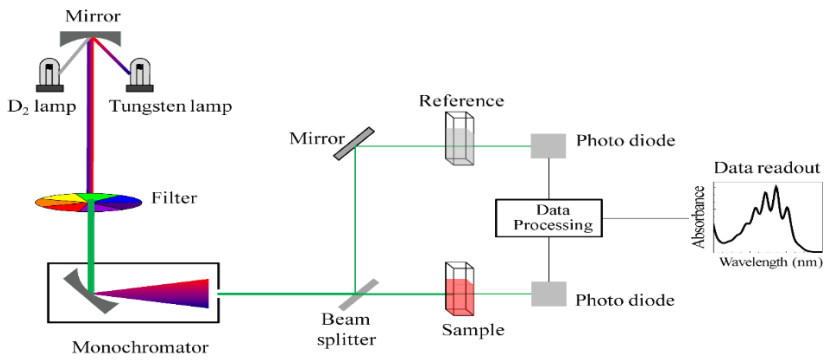

Figure 1.12 Schematic illustration of UV/visible spectrometer

The UV / Vis spectrometer absorption spectrum ranges from 200 nm to 800 nm. The spectrometer includes a double beam with strong resolving power along with a double pass monochromator.

The light beam of the Deuterium lamp moves from the filter and a concave mirror focusing on a grating. Grating reflects this beam again. The reflected beam is then directed to a partial reflective mirror dividing the beam further to two routes. One beam passes from the specimen while the other from the reference material and lastly focusing on the detector. This scheme is illustrated in **figure 1.12.**

1.10 Objectives of this work

This thesis addresses an attempt to generate TiO_2/GO nanocomposites. The purpose of nanocomposite synthesis is to create a photocatalyst that is visible light active and has improved photocatalytic activity for dye degradation.

Following are detailed objectives of this thesis:

1. Synthesis of TiO_2 nanoparticles by sol-gel method.
2. Synthesis of N-doped and N/Zn co-doped TiO_2 nanoparticles by sol-gel method.
3. Characterization of all prepared samples.
4. Choosing the best catalyst by performing degradation studies of Methyl Orange.
5. Synthesis of Graphene oxide nanosheets by Hummers' method.
6. Synthesis of nanocomposite of Graphene Oxide and the as prepared best catalyst by hydrothermal method.
7. Performing degradation studies and comparing the results.

2 LITERATURE REVIEW

This section includes all the literature reviewed before and during the research. Much study has been performed on the synthesis of nanoparticles and their doping, synthesis of nanocomposites and degradation of various types of dyes. This thesis involves the literature on the synthesis of TiO_2, its doping, its composite formation and methyl orange degradation involving these photocatalysts.

2.1 Nanoparticles of TiO_2

In 1972, by using TiO_2 semiconductor, Fujishima and Honda observed the water splitting phenomena [33].Since that finding, TiO_2 has been widely used for photocatalytic activity in various morphologies. Of all the other morphologies, TiO_2 nanoparticles have established to be the best photocatalytic activities [34]. In 1977, Frank and Bard used technology of water splitting to reduce cyanide ion [35].TiO_2 nanoparticles have increased surface area, so the use of them is included in this work. Many techniques have been used to date for the production of TiO_2 nanoparticles. But among all these techniques, sol-gel has been validated to be the best for nanoparticles production.

Chen-Chi Wang and Jackie Y. Ying (1999), described the production of TiO_2 nanoparticles for first time via sol-gel technique. They studied all optimum conditions and parameters for the creation of highly fine, nano-sized and non-agglomerated particles. They investigated the heat treatment as well, as this influenced the particles' crystallinity. This technique was used to obtain nanoparticles up to 6 nm size in anatase form by regulating all parameters [36].

Huaming Yang, Ke Zhang and Rongrong Shi (2006), stated the sol-gel synthesis route for TiO_2 nanocrystal preparation and their photocatalytic study for the degrad ation of methyl orange. Calculated from XRD study, the crystal size was nearly 16 nm and the calcination temperature was maintained at 500 ºC. The temperature rise from 500 ºC showed both the features of anatase and rutile phase. Studies of anatase-phase methyl orange degradation showed better outcomes than the rutile phase. The photodegradation

rate of methyl orange was also impacted by pH control, hydrogen peroxide addition and TiO_2 reusability [37].

M. Hamadanian, A. Reisi-Vanani and A. Majedi (2010), reported TiO_2, Cobalt doped TiO_2 nanoparticles synthesized by sol-gel route including ultra-sonication treatment. For all the samples that were prepared, anatase stage was achieved. The TiO_2 nanoparticles and those doped with cobalt were verified by all the characterization methods that were conducted [38].

R. Vijayalakshmi and V. Rajendran (2012), reported synthesis of TiO_2 nanoparticles through sol-gel and hydrothermal techniques. TiO_2 nanoparticles produced by the sol-gel technique were more crystalline and had almost 7 nm of crystallite size. Whereas, the crystallite size of TiO_2 nanoparticles generated by hydrothermal processing was nearly 17 nm, much greater than the earlier technique. Bandgap for both sizes relied on the size of the crystallite [39].

Ajay Sharma, R.K. Karn and S.K. Pandiyan (2014), reported the production of nanostructured TiO_2 from sol-gel method by simple hydrolysis of Titanium Isopropoxide. The prepared nanoparticles had about 20 nm of crystallite size. The combination of anatase and rutile phase nanoparticles was verified using XRD method. The morphology and particle size of samples was studied using SEM. Only the anatase phase showed spherical morphology. For this phase, the calculated band gap was about 3.2 eV [40].

Raad S. Sabry, Yousif K. Al-Haidarie and Muhsin A. Kudhier (2016), reported the successful production of anatase phased TiO_2 nanoparticles using $TiCl_4$ as precursor. This technique is cost-effective and is a simple approach executed at room temperature. When TiO_2 was calcined at a greater temperature and the duration of gel formation expanded, the size of the crystallite was also enhanced and verified by XRD information. Degussa-P25 showed reduced performance, while sol-gel synthetic TiO_2 nanoparticles showed enhanced performance for methylene blue degradation. The greater surface area of nanoparticles contributed to the enhanced performance [41].

2.2 Nitrogen doped TiO_2 nanoparticles

M. Sathish, B. Viswanathan and R. P. Viswanath (2004), described the synthesis of nitrogen doped TiO_2 nanoparticles by means of simple chemical route and calcination temperature of 400 ºC. The nanoparticles produced were roughly 14 nm homogeneous in size and were in spherical form. For two particular reasons, this technique was more effective than other techniques: (i) Low price technique and precursors were used to synthesize TiO_2 nanoparticles doped with nitrogen. (ii) Resulting TiO_2 nanoparticles were uniform in size and shape. N-doped TiO_2 nanoparticles showed better photocatalytic activity below visible light for methylene blue degradation than Degussa-P25 and pure TiO_2 nanoparticles [42].

Yu Huan, Zheng Xuxu and Yin Zhongyi (2007), described the successful production of nitrogen doped TiO_2 nanoparticles with sol-gel treatment. As a source of nitrogen, ammonium chloride was used and calcination was conducted at particular temperatures. The studies showed the impact of pH and particular calcination temperatures on nanoparticles particle size, which also impacted the photocatalytic activity as a whole. Perfect outcomes were achieved for photocatalytic activity when calcination temperature was sustained at 500 ºC and pH was kept at 3. The nitrogen-doped TiO_2 nanoparticles showed improved activity for 4-chlorophenol degradation below visible light than undoped TiO_2 nanoparticles [43].

J. Senthilnathan and Ligy Philip (2010), reported the photocatalytic action using nitrogen doped TiO_2 nanoparticles in irradiated visible light. Modified sol-gel technique has been utilized to make these doped photocatalysts for TiO_2 nanoparticles. Triethylamine has been used in TiO_2 nanoparticles as a nitrogen precursor for doping. Different characterization verified nitrogen doping and XRD performance calculations gave approximately 22 nm of crystalline size. In this research, XPS information showed that oxygen atom was swapped by nitrogen atom in TiO_2 lattice. Prepared photocatalyst used visible light irradiation to degrade Lindane. The highest outcomes for degradation were shown by N-doped TiO_2 nanoparticles. Lindane was totally degraded and verified by analyzing GC-MS [44].

Armineh Hassanvand, Morteza Sohrabi and Sayed Javid Royaee (2014), reported synthesis of nitrogen doped TiO_2 nanoparticles via simple and direct impregnation technique by applying amination over bulk TiO_2 (Degussa-P25). Using different techniques, these doped TiO_2 nanoparticles were characterized. These methods verified the existence in the prepared nanoparticles of both anatase and rutile stages. Comparison of both the prepared catalyst and bulk TiO_2 in visible light treatment was examined by the degradation of phenol. TiO_2 nanoparticles with nitrogen doping displayed increased photocatalytic activity relative to TiO_2 bulk [45].

Aboubakr M. Abdullah, Noora J. Al-Thani and Khouloud Tawbi (2016), reported the production of carbon and nitrogen co-doped on TiO_2 and carbon tetrachloride and polyaniline were used respectively as precursors. The calculated particle size was between 35 nm and 40 nm from SEM illustrations. The incorporation of nitrogen and carbon were confirmed by different characterization methods. The photocatalyst prepared showed enhanced performance for phenol degradation below UV light irradiation than bulk TiO_2 and pure TiO_2 [46].

2.3 Zinc and nitrogen co-doped TiO_2 nanoparticles

Zhang, H., Liang, Y., Wu, X., & Zheng, H. (2012), reported the sol-gel production of zinc and nitrogen co-doped TiO_2 nanoparticles. Different characterization techniques were performed and incorporation of zinc and nitrogen both were confirmed. Patterns of transmission electron microscopy (TEM) disclosed that the typical grain size of all samples was about 15 nm and an apparent aggregation of particles was caused because of zinc doping. (Zn, N)-doped TiO_2 with 1 at. % Zn doping level, showed best photocatalytic activity for methylene blue (MB) degradation [47].

Aware, D. V., & Jadhav, S. S. (2016), reported the production of zinc doped TiO_2 nanoparticles by surfactant-assisted sol-gel technique. Creation of anatase phase of TiO_2 and crystallite sizes in the range of 12.6-18.1 nm were confirmed using XRD. Zinc doping along with the small crystallite size hindered phase transformation and promotes anatase phase growth. Spherical morphology of nanoparticles with a diameter of 12-18 nm was confirmed with SEM and TEM techniques. A decrease in band gap of TiO_2 was observed because of doping. Methyl red was degraded for the study of the photocatalytic activity of

the manufactured nanoparticles. The degradation studies exhibited greater activity of doped samples in comparison with the undoped ones. The small grain size, increased crystallinity, increased specific surface area and a reduction in doped nanoparticle's band gap may be accountable for the increased photocatalytic activity[48].

Rimoldi, L., Pargoletti, E., Meroni, D., Falletta, E., Cerrato, G., Turco, F., & Cappelletti, G. (2018), reported the comparison between tin and zinc as metal dopants for nitrogen and metal co-doped TiO_2 nanoparticles to improve the photocatalytic absorption of TiO_2 nanoparticles. Tetracycline was used for the degradation studies. Increased photocatalytic activity was shown by codoped samples in comparison with the pure and N-doped TiO_2 nanoparticles. The increased photocatalytic activity is credited to modified phase composition and enhanced surface area [49].

Wattanawikkam, C., & Pecharapa, W. (2015), reported the successful creation of zinc doped TiO_2 nanoparticles and their comparison to bare TiO_2 nanoparticles. The resulting nanoparticles had particle size ranging from 10-15 nm as displayed by TEM images. The band gap of TiO_2 extended into visible region due to addition of Zn atoms. The optical properties of TiO_2 nanomaterials was greatly affected by Zn doping [50].

Yu, Y., Wang, J., Li, W., Zheng, W., & Cao, Y. (2015), reported the synthesis of a series of zinc doped TiO_2 nanoparticles with varying concentrations of zinc via sol-gel technique and via annealing at varying temperatures. It was observed that Zn^{2+} existed only as surface species (O-Zn-Cl or $ZnTiO_3$) other than be doped within TiO_2 lattice. Introduced Zn^{2+} ions first existed as O-Zn-Cl on the surface of TiO_2. As the calcination temperature increased, the O-Zn-Cl transferred into $ZnTiO_3$. Rise of introduced Zn content is advantageous for the creation of $ZnTiO_3$. Presence of $ZnTiO_3$ induced the formation of rutile phase that resulted in decreased temperature for phase transition [51].

2.4 Graphene oxide

Karthikeyan Krishnamoorthy, Rajneesh Mohan, and S. J. Kim (2011), reported the photocatalytic activity of graphene oxide. Graphene oxide synthesis was conducted through adjusted technique of Hummers' and characterization methods verified the existence of oxygen groups on the graphene sheet surface. Graphene oxide's photocatalytic activity was noted by reducing resazurin to resorufin and changing their color from blue to

pink as well. The reduction was made by the electrons on the graphene sheet surface when UV light irradiated them [52].

William S. Hummers, Jr. and Richard E. Offeman (1957), reported for first time, the production of graphite oxide by Hummers' process. By adding graphite flakes and $NaNO_3$ to concentrated H_2SO_4, graphite oxide was prepared. The resulting solution was held in a battery container that was kept under constant stirring at 0ºC temperature. Graphite was then oxidized by slow addition of $KMnO_4$. Then the temperature was raised for half an hour to 35 ºC. Water was then introduced slowly, resulting in temperature increase of up to 98 ºC. More water was added and then H_2O_2 was used to stop the reaction. Separation of the graphitic layers was achieved by filtration and washing. Graphite oxide powder was obtained after drying at 40 ºC. This technique generated a large quantity of graphite oxide [53].

Ji Chen, Bowen Yao, Chun Li and Gaoquan Shi (2013), introduced the eco-friendly technique for the production of graphene oxide by altering already given hummers' process. To prevent the release of toxic and dangerous gases, they removed sodium nitrate from the standard Hummers' process. This method proved to be more environment friendly as well as cheap, and the wastewater treatment was made even easier. In this method, graphite flakes were straight added to sulfuric acid and in the presence of ice bath, constant stirring was achieved. Potassium permanganate was then slowly added for graphene oxidation. Water addition was done and hydrogen peroxide stopped the reaction.

Graphene oxide sheets were gained after washing by hydrochloric acid and water and then drying [54].

Leila Shahriary and Anjali A. Athawale (2014), described the production of graphene oxide sheets by altered Hummers' process. This technique involved adding concentrated sulfuric acid to graphite flakes and sodium nitrate in a constant stirring beaker. After one hour, potassium permanganate was added for graphene oxidation. This blend was stirred for 12 hours and then addition of water was done with vigorous stirring. To finish the reaction, hydrogen peroxide was added at the end. The blend obtained was handled by hydrochloric acid washing and distilled water and sheet drying [55].

Paulchamy B, Arthi G and Lignesh BD (2015), described the production of graphene oxide by hummers' process and altered hummers' process. This method involved adding $NaNO_3$ and H_2SO_4 to graphite powder for 2 hours under constant stirring and maintaining up to 5° at low temperature. Slow addition of $KMnO_4$ after 2 hours of stirring was done. The temperature was maintained at 35° with continuous stirring for 2 days. A gray slurry was developed after 2 days of stirring. Water was added gently and then shifted to add H_2O_2 addition to stop the reaction. The solution obtained is settled and decanted, sonicated, washed with HCl and water. It was then dried to obtain graphene oxide in a vacuum oven for 24 hours. By different characterization techniques, especially XRD and FTIR analysis, oxygen functional group on graphene sheets' surface was confirmed. SEM images confirmed the exfoliation of graphite into graphene sheets [56].

2.5 Graphene oxide/ TiO_2 nanocomposites

N.R. Khalid, E. Ahmed and Zhanglian Hong (2012), reported the production of nitrogen doped TiO_2 nanoparticles decorated on graphene oxide sheets via hydrothermal process. This research showed that all prepared nanocomposites had improved photocatalytic activity comparative to plain TiO_2 nanoparticles for methyl orange degradation. When nitrogen doping and graphene oxide composites were created as shown in **Figure 2.1**, bandgap narrowing was observed, electron-hole separation was detected and methyl orange adsorptivity improved owing to the big particular graphene sheet surface area [57].

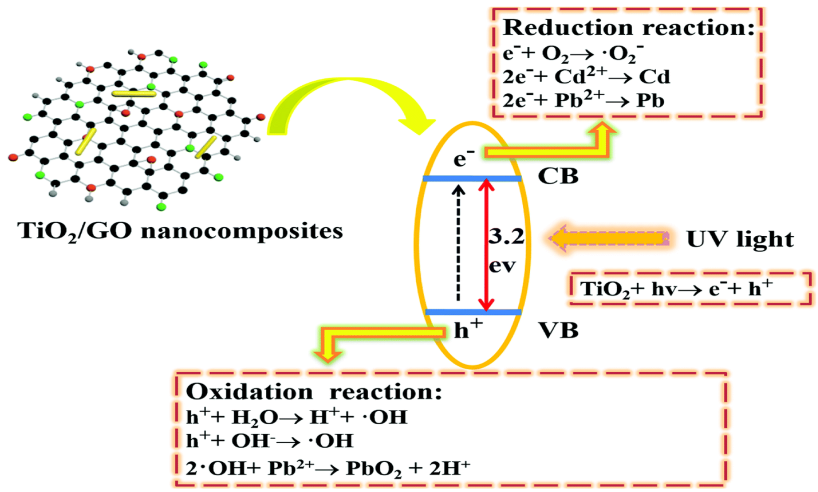

Figure 2.1 Photocatalytic activity of N-doped TiO_2/ GO composite

N. R. Khalid, E. Ahmed and Zhanglian Hong (2013), reported the production of copper doped TiO_2 nanoparticles/ graphene oxide nanocomposite via hydrothermal process. In comparison with pure TiO_2 nanoparticles, the photocatalytic activity experiments showed enhanced photoactivity for methyl orange degradation while using nanocomposites. The efficiency was enhanced owing to segregation of the electron-hole and improved nanocomposite adsorptivity owing to sheet-like graphene oxide composition. There was more interaction between graphene oxide nanocomposite and the dye to be degraded, confirming the increased activity [58].

XiaopengShanga, Min Zhanga and Yingkui Yang (2014), reported the production of sulphur and nitrogen co-doped TiO_2 nanoparticles/ graphene oxide nanocomposites by easy hydrothermal process. When exposed to UV light, prepared nanocomposites showed greater photocatalytic activity for methyl orange degradation. Graphene oxide generated an rise in photocatalytic activity because of its wide surface area. Graphene oxide also hinders electrons transfer and reduces the risk of recombination of electron-holes [59].

Hemraj M. Yadav and Jung-Sik Kim (2016), reported the production of TiO_2 nanoparticles/ graphene oxide nanocomposites having various concentrations of graphene oxide via solvothermal process. XRD data, TEM analysis and photoluminescence spectroscopy recognized graphene oxide sheets. SEM assessment verified the existence of TiO_2 nanoparticles on graphene oxide sheets. Compared to pure TiO_2 nanoparticles, the composites prepared gave improved photocatalytic activity for benzene gas degradation. This improved activity was because of the reduced recombination of charge [60].

3 EXPERIMENTAL WORK

This section includes the information of the chemicals used in this work and the experimental procedure. In addition, at the end of this section, different characterization methods used to evaluate the sample were also discussed shortly.

All chemicals used to synthesize the desired catalysts and composites are analytical grade and no further refinement has been required.

3.1 Synthesis of TiO_2 nanoparticles

Sol-gel technique has been utilized for TiO_2 nanoparticles preparation. Titanium (IV) isopropoxide (97%) was utilized as a TiO_2 precursor and Urea and Zinc acetate were used as nitrogen and zinc precursors for doping.

3.1.1 Chemicals

Titanium (IV) isopropoxide (97%) (Sigma Aldrich), Nitric acid (Sigma Aldrich) and 2-propanol (Sigma Aldrich).

3.1.2 Procedure

5 ml of Tetra Titanium isopropoxide (TTIP) was added in a beaker with 6 ml of 2-propanol for the synthesis of TiO_2 nanoparticles and stirred for 15 min. 2-3 drops of nitric acid have been added in another beaker in 80 ml of water to achieve the pH to 3. In vigorous continuous stirring, the previously prepared solution of TTIP and 2-propanol was then drop-wise added to this water. Then this solution was stirred overnight. This solution was dried in a vacuum oven for 8h at temperature under 80°C after one night. The dried solid particles that were collected were then ground into fine powder. To acquire anatase form of TiO_2 nanoparticles in white powder form. This powder was further calcined at 450°C for 8 h.

The same method was used for nitrogen and zinc doping. The percentage of nitrogen was kept the same as in the literature, but the concentrations of zinc was varied.

3.2 Synthesis of nitrogen doped TiO_2 nanoparticles

3.2.1 Chemicals

Titanium (IV) isopropoxide (97%) (Sigma Aldrich), Zinc acetate ($Zn(CH_3CO_2)_2$) (Sigma Aldrich), Nitric acid (Sigma Aldrich) and 2-propanol (Sigma Aldrich).

3.2.2 Procedure

For nitrogen doping, 3 g of urea was added to water containing 2-3 drops of nitric acid and TTIP and 2-propanol were then added dropwise. The blend was stirred overnight, vacuum-dried for 8h and calcined at 450°C and a yellow powder was acquired.

3.3 Synthesis of zinc and nitrogen co-doped TiO_2 nanoparticles

3.3.1 Chemicals

Titanium (IV) isopropoxide (97%) (Sigma Aldrich), Zinc acetate ($Zn(CH_3CO_2)_2$) (Sigma Aldrich), Urea (Merck), Nitric acid (Sigma Aldrich) and 2-propanol (Sigma Aldrich).

3.3.2 Procedure

For co-doping with nitrogen and zinc, 3 g of urea with 0.1% (4.7mg), 0.5% (23mg), 1% (47mg) and 2% (95mg) of zinc acetate were added individually in water containing nitric acid and 4 solutions were prepared. Drop-wise addition, stirring overnight, drying at 80°C and calcination at 450°C resulted in light yellow colored powder based on the proportion of zinc used.

The products obtained before and after calcination had different color transitions. Also the colors of different samples with different percentages were also varying according to the amount of Zn percentage.

3.4 Synthesis of graphene oxide

Graphene oxide nanosheets were produced using Hummers' method using graphite powder as a precursor.

3.4.1 Chemicals

Graphite powder (Sigma Aldrich), Sodium Nitrate (BDH), Potassium permanganate (Sigma Aldrich), Hydrogen peroxide (Merck), Sulfuric acid (95 %) (Sigma Aldrich), Hydrochloric acid (37 %) (Sigma Aldrich).

3.4.2 Procedure

2 g of graphite flakes in 1000 ml beaker were taken. 50 ml of H_2SO_4 (98 %) was added in it, reaction blend was kept at 0-5 ºC in ice bath under continuous stirring. To create defects, 2 g of $NaNO_3$ was added gradually. Reaction blend was stirred at 0-5 ºC till 2h. To oxidize graphite flakes, 6g of $KMnO_4$ was added slowly and kept at max 15 ºC temperature.

The ice bath was then removed. Temperature was maintained at 35 ºC. The resultant brownish mixture was stirred for 2 days. Gradual addition of 100 ml of H_2O was done to dilute reaction mixture. Rapid increase in reaction temperature (up to 98 ºC) appeared with effervescence. Addition of water changes the color of slurry from grey to brown. Under continuous stirring, the reaction mixture was further diluted with 200 ml of H_2O. To terminate the reaction, drop-wise addition of 10 ml of H_2O_2 was done that gave yellow color to the reaction blend. The reaction mixture was then washed with 10 % HCl and five times with deionized water. Obtained gel like material was then dried in vacuum oven at 60 ºC to obtain GO powder.

3.5 Synthesis of GO/Zn-N co-doped TiO_2 nanocomposite

The best catalyst after the degradation analysis of dye using co-doped TiO_2 was chosen and its nanocomposite with already prepared GO was prepared to further improve the photocatalytic characteristics and verify its degradation capacity. For their preparation, hydrothermal technique was used.

3.5.1 Chemicals and materials

As prepared best selected nitrogen and zinc co-doped TiO_2 nanoparticles and graphene oxide.

3.5.2 Procedure

Three ratios of GO/TNPs were taken to study the degradation of dye. Graphene oxide (0.5:1, 1:1 and 2:1) was distributed in 30 ml of deionized water by probe sonicator separately in 3 different beakers.

After 30 minutes of sonication same amount of best selected co-doped TiO_2 nanoparticles powder was added in to each of the three beakers and again sonication was done at low

amplitude. Then vigorous stirring was done for 3 hours. The prepared suspensions were transferred to autoclaves and held at 120 ^{0}C till 4 hours. Products obtained were then washed with deionized water several times and dried under vacuum at 60 ^{0}C. Powder form of samples was obtained.

Table 3.1 Details of TiO_2 and doped-TiO_2 photocatalysts

Sample ID	Composition	Dopant %age	Annealing Temp.
T	TiO_2	0%	450 ºC
NT	Nitrogen doped TiO_2	3-N	450 ºC
0.1%Zn-NT	Zinc and Nitrogen co-doped TiO_2	3-N, 0.1%-Zn	450 ºC
0.5%Zn-NT	Zinc and Nitrogen co-doped TiO_2	3-N, 0.5%-Zn	450 ºC
1%Zn-NT	Zinc and Nitrogen co-doped TiO_2	3-N, 1%-Zn	450 ºC
2%Zn-NT	Zinc and Nitrogen co-doped TiO_2	3-N, 2%-Zn	450 ºC

Table 3.2 Details of GO/TiO_2 nanocomposites

Sample ID	Composition	Amounts
0.5:1-GO/T	Graphene Oxide, Zinc and Nitrogen co-doped TiO_2	50 mg GO, 100 mg 2% Zn-NT
1:1-GO/T	Graphene Oxide, Zinc and Nitrogen co-doped TiO_2	100 mg GO, 100 mg 2% Zn-NT
2:1-GO/T	Graphene Oxide, Zinc and Nitrogen co-doped TiO_2	200 mg GO, 100 mg 2% Zn-NT

4 RESULTS AND DISCUSSION

This section contains all methods of characterization conducted and all outcomes from various experiments.

4.1 Characterization

Structural investigation of all the synthesized samples was carried out by X-ray Diffraction (XRD) data, Scanning Electron Microscopy **(**SEM) analysis, Energy Dispersive X-ray Spectroscopy (EDS) data and UV/Visible-DRS data.

4.1.1 XRD

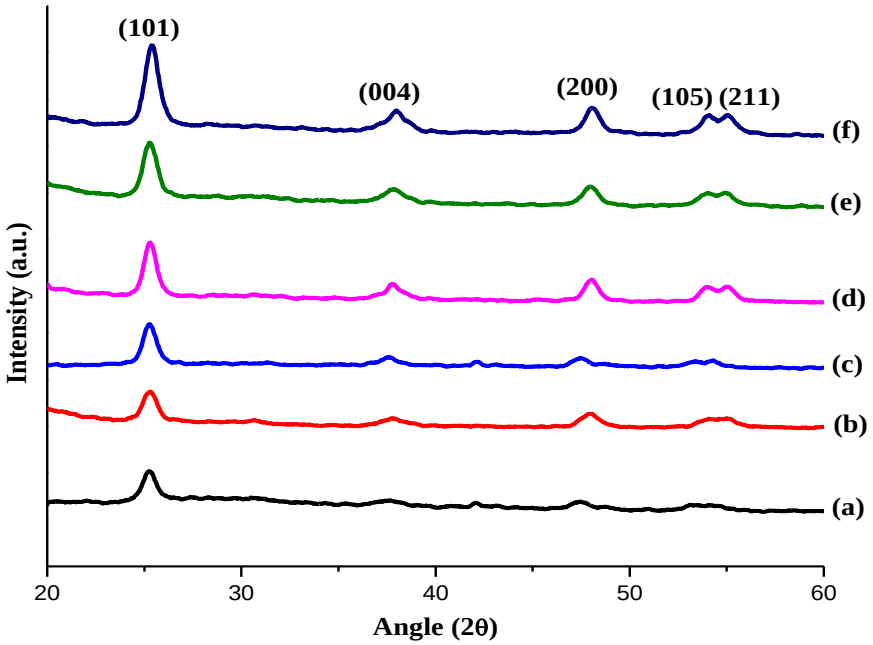

Figure 4.1 XRD peaks of prepared nanoparticles showing: **(a)** Pure TiO_2 **(b)** N- TiO_2 **(c)** 0.1% Zn-NT **(d)** 0.5% Zn-NT **(e)** 1% Zn-NT **(f)** 2% Zn-NT

XRD machine used for this study was JSX 3201, Jeol, Japan existing at School of Chemical and Material Engineering, NUST, Islamabad. JCPDS No.21-1272 clearly matches with all the obtained XRD results of prepared nanoparticles and the absence of impurity peaks also confirms phase purity. TiO_2 anatase is in highly crystalline form which can be observed from narrow and sharp peaks. Diffraction peaks appeared at 25.36°, 37.84°, 48.08°, 53.94° and 55.08° having lattice planes at (101), (004), (200), (105) and (211) respectively. The dopant elements nitrogen and zinc do not show peaks

because of low concentration but a slight shift of peaks due to doping can be perceived in **Figure 4.1** and clearly in **table 4.1**. This is on account of incorporation of Zn and N ions within TiO_2 lattice that causes a change in cell volume and cell parameters of TiO_2 crystal lattice. Characteristic rutile peaks were not observed as pure anatase phase was formed and is confirmed.

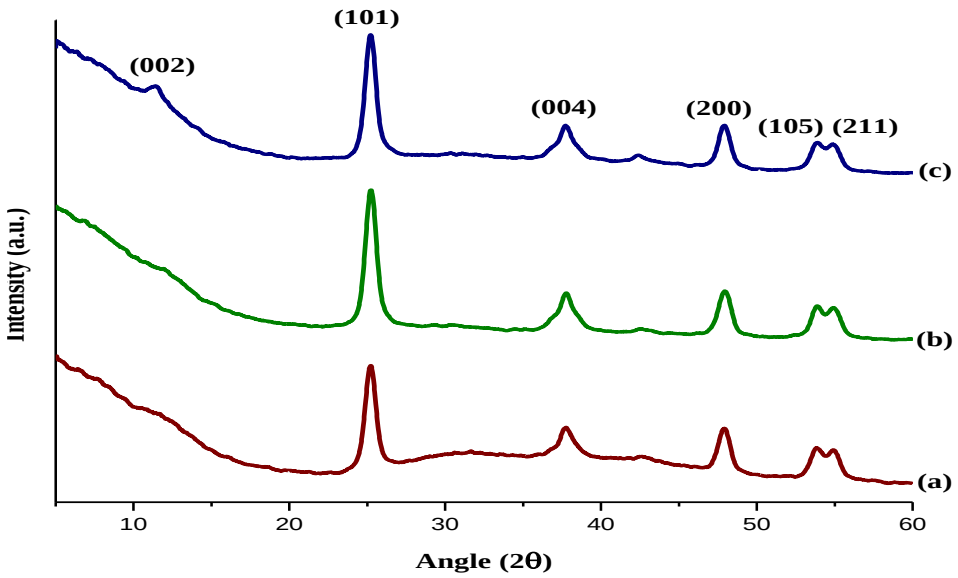

Figure 4.2 XRD peaks of prepared nanocomposites showing: **(a)** 0.5:1 GO-T **(b)** 1:1 GO-T **(c)** 2:1 GO-T

In **figure 4.2**, the anatase phase of 2% Zn/N co-doped TiO_2 nanoparticles can be clearly seen and crystallinity of samples can be confirmed by increased intensity of peaks and decreased broadening. Moreover, this figure shows the results of the nanocomposites GO and the prepared catalyst with different ratios (0.5:1, 1:1 and 2:1). The characteristic peak of GO which appears at 10.7° having lattice plane at (002), can be seen in all the composites with increase in intensity by increasing the concentration of GO. The crests are also moved from their location due to composite formation.

Average crystallite size of all the synthesized catalysts was calculated by Scherrer equation:

$$D = k\lambda / \beta \cos\theta$$

Where,

D = Crystallite size

k = Scherrer constant

λ = Wavelength of x-rays utilized (Cu k-alpha are typically used having **λ** of 0.15405 nm)

β = Full width half maximum (FWHM) of observed peak

θ = Diffraction angle in degrees

Pure TiO_2 has crystallite size of 20 nm and doping lowers the size up to 5.4 nm. This lowering of crystallite size with increase in dopant concentration can be clearly observed in **table 4.1.**

Table 4.1 Average crystallite size of all synthesized catalysts and composites

Sample ID	Peak Position	FWHM	Crystallite size of peak (nm)	Average crystallite size (nm)
T	25.26	0.39	20.64	19.6
	37.64	0.48	17.29	
	47.46	0.55	15.60	
	53.16	0.41	21.20	
	54.1	0.38	23.21	
NT	25.22	0.73	10.91	17.1
	37.58	0.60	13.69	
	47.88	0.39	21.83	
	54.72	0.47	18.54	
	55.06	0.43	20.44	
0.1%Zn-NT	25.37	0.66	12.11	16.0
	37.95	0.34	23.92	
	48.18	0.46	18.62	
	53.76	0.57	15.23	
	54.93	0.63	13.83	
0.5%Zn-NT	25.18	0.80	10.04	15.2
	37.82	0.41	20.06	
	47.96	0.61	13.93	
	53.8	0.36	24.46	

	55.1	0.84	10.47	
1%Zn-NT	25.33	0.62	12.98	14.3
	37.77	0.62	13.39	
	48.10	0.71	12.11	
	53.90	0.42	20.98	
	54.93	0.75	11.80	
2%Zn-NT	25.32	0.73	10.93	13.0
	37.86	0.63	13.13	
	48.14	0.80	10.66	
	54.06	0.57	15.28	
	55.1	0.57	15.51	
0.5:1 GO-T	10.44	3.92	2.00	5.9
	24.78	0.94	8.53	
	37.32	4.38	1.89	
	47.51	1.19	7.17	
	53.38	1.17	7.46	
	54.49	1.03	8.50	
1:1 GO-T	12.01	1.02	7.74	5.7
	25.25	2.42	3.32	
	37.79	3.05	2.72	
	47.94	1.01	8.47	
	53.85	2.16	4.07	
	54.96	1.09	8.11	
2:1 GO-T	11.46	3.60	2.19	5.4
	25.15	4.74	0.32	
	37.73	2.11	3.92	
	47.94	1.03	8.34	
	53.91	1.08	8.09	
	54.85	1.05	8.41	

4.1.2 SEM

SEM utillized in this study for characterization of sample is JSM-6490A, JEOL-Japan, existing at School of Chemical and Materials Engineering, NUST, Islamabad. Morphology of unaltered TiO_2 was sphere-shaped but doped particle become more like aggregated plates. Agglomeration was also seen in samples that were probably because of nucleation during hydrolysis or heat treatment.

Zn doping affects the catalyst by decreasing grain size and in turn increasing the surface area which leads to increased photocatalytic activity. **Figure 4.3** shows spherical morphology of all the prepared catalysts and increase in agglomeration with increase in zinc content. Zinc plates can also be seen in the prepared catalysts, especially is 2% Zn/N co-doped TiO_2 nanoparticles as it contains the highest amount of zinc.

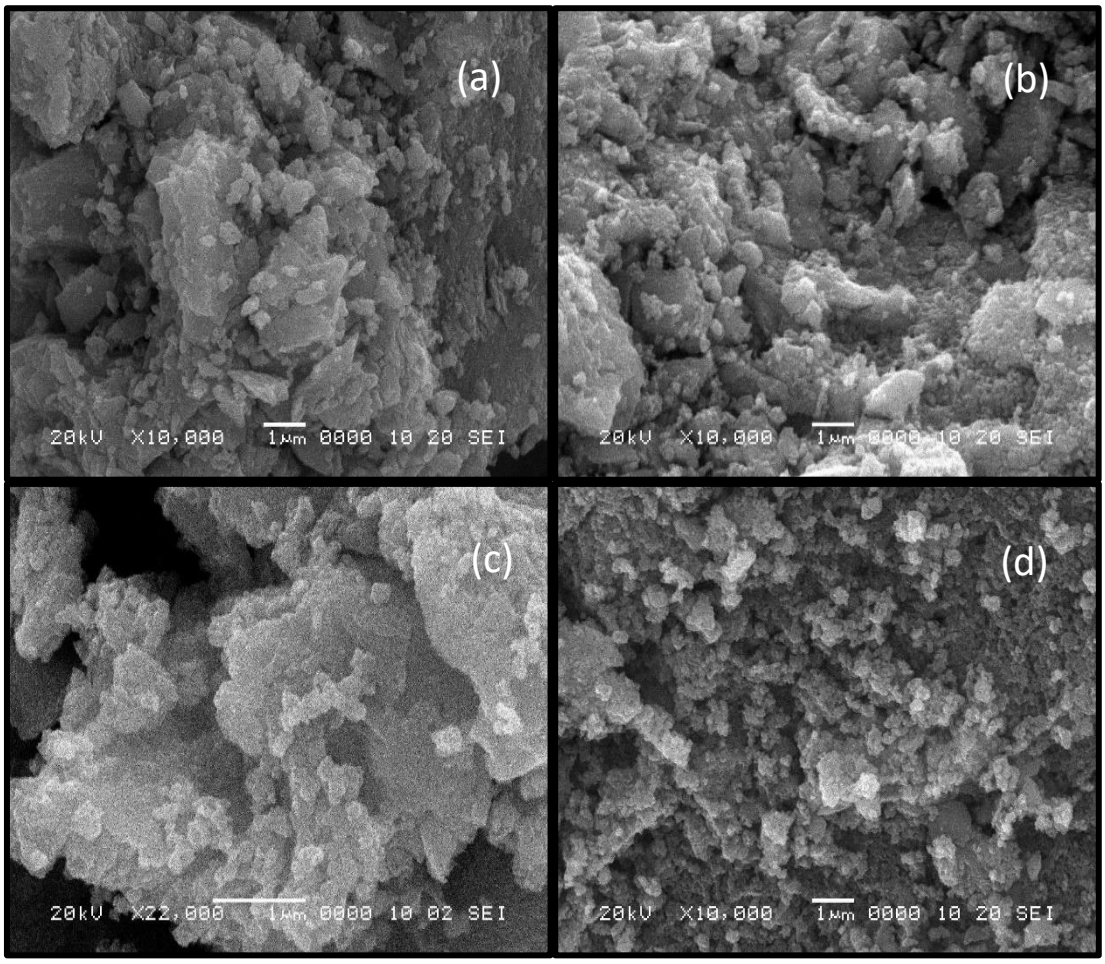

Figure 4.3 SEM images: (a) 0.1% Zn-NT (b) 0.5% Zn-NT (c) 1% Zn-NT (d) 2% Zn-NT

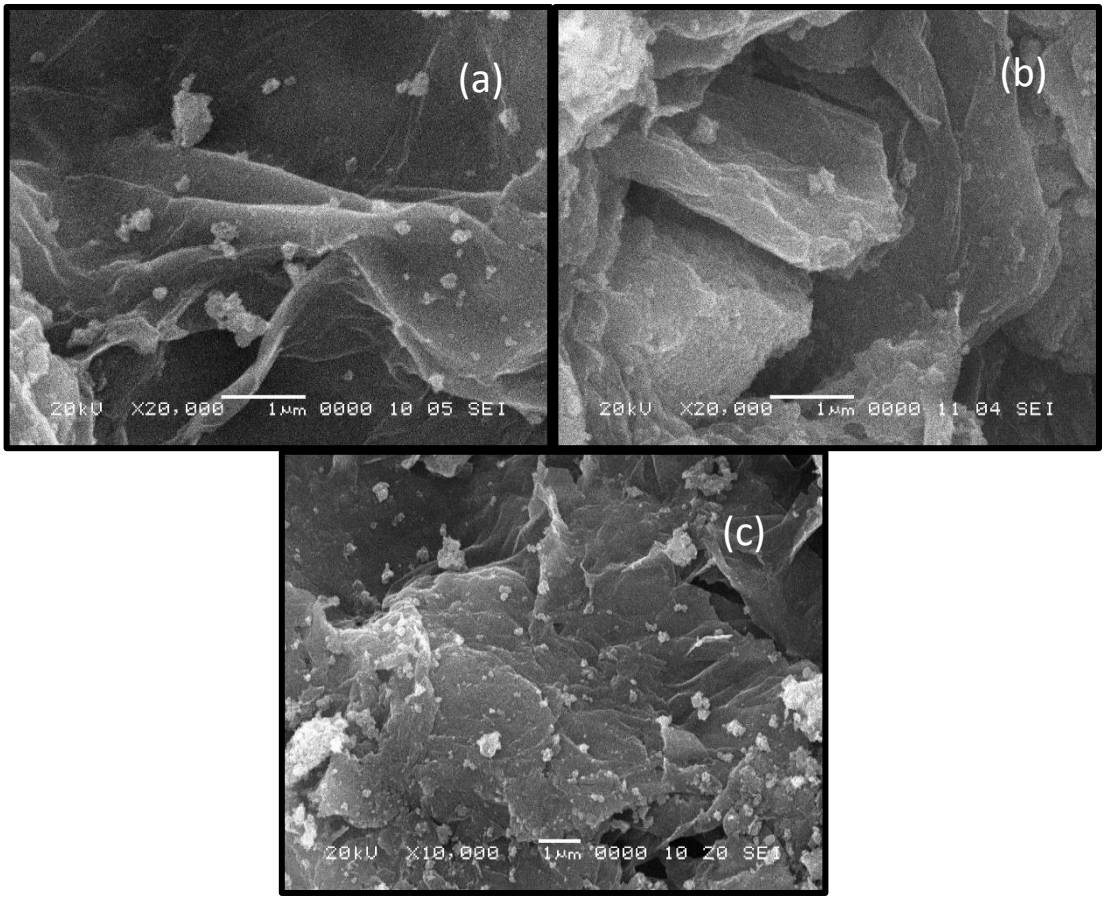

Figure 4.4 SEM images: **(a)** 0.5:1 GO-T **(b)** 1:1 GO-T **(c)** 2:1 GO-T

Figure 4.4 (a), **(b)** and **(c)** displays incorporation of Zn/N co-doped TiO_2 nanoparticles on GO sheets. The particle size of all the prepared catalysts and composites is shown in **table 4.2** and it is visible that rise in dopant concentration has decreased the particle size from 35 nm to 6 nm.

Table 4.2 Average particle size of all prepared samples

Sample ID	Average particle size (nm)	Sample ID	Average particle size (nm)
0.1%Zn-NT	32.07	**0.5:1-GO/T**	10.59
0.5%Zn-NT	30.15	**1:1-GO/T**	11.84
1%Zn-NT	29.68	**2:1-GO/T**	8.82
2%Zn-NT	17.78	--	--

4.1.3 EDS

EDS is utilized for the elemental configuration detection of the sample. Each element show specific peak in the graph depicting its presence in the sample. TESCAN machine present at USPCAS-E, NUST was used for EDS analysis**. Figure 4.5** shows EDS analysis of all the prepared catalysts. Zinc peaks are clearly seen in **figure 4.5 (a)**, **(b)**, **(c)** and **(d)** according to their concentrations along with Ti and O peaks.

EDS results obtained for each prepared sample exactly shows the amount of each element that is either already present or is doped. The amount of zinc that is varied from 0.1% to 2% is clearly seen in the weight percentages in **table 4.3**. Nitrogen content cannot be seen in each sample as the weight of nitrogen is very low and its amount cannot be observed.

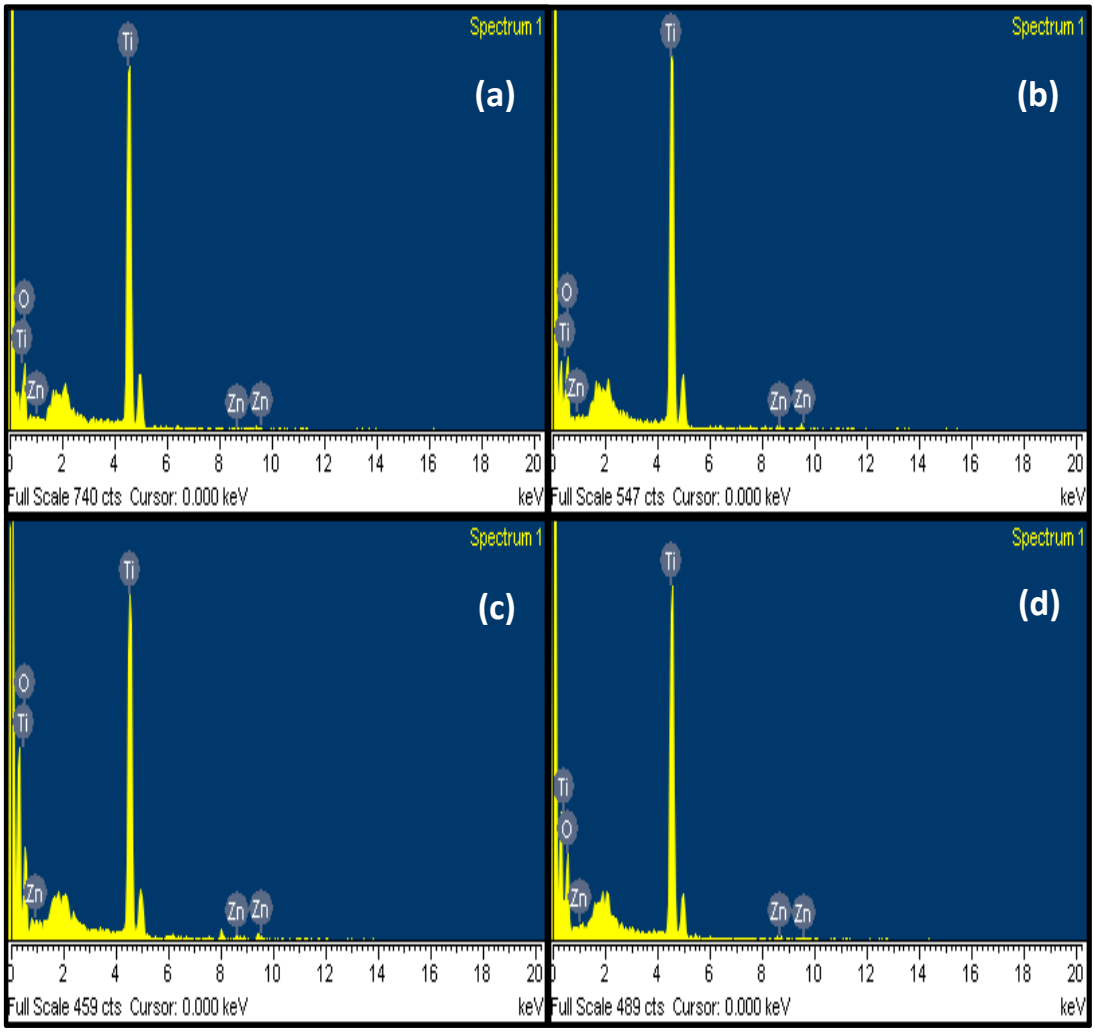

Figure 4.5 EDS analysis: **(a)** 0.1% Zn-NT **(b)** 0.5% Zn-NT **(c)** 1% Zn-NT **(d)** 2% Zn-NT

Table 4.3 EDS results: (a) 0.1% Zn-NT (b) 0.5% Zn-NT (c) 1% Zn-NT (d) 2% Zn-NT

Element	Weight%	Atomic%
O K	43.14	69.47
Ti K	56.53	30.41
Zn K	0.33	0.13
Totals	100.00	**(a)**

Element	Weight%	Atomic%
O K	41.80	68.36
Ti K	57.18	31.23
Zn K	1.02	0.41
Totals	100.00	**(b)**

Element	Weight%	Atomic%
O K	48.01	74.11
Ti K	50.21	25.24
Zn K	1.78	0.65
Totals	100.00	**(c)**

Element	Weight%	Atomic%
O K	47.13	72.98
Ti K	50.57	26.15
Zn K	2.30	0.87
Totals	100.00	**(d)**

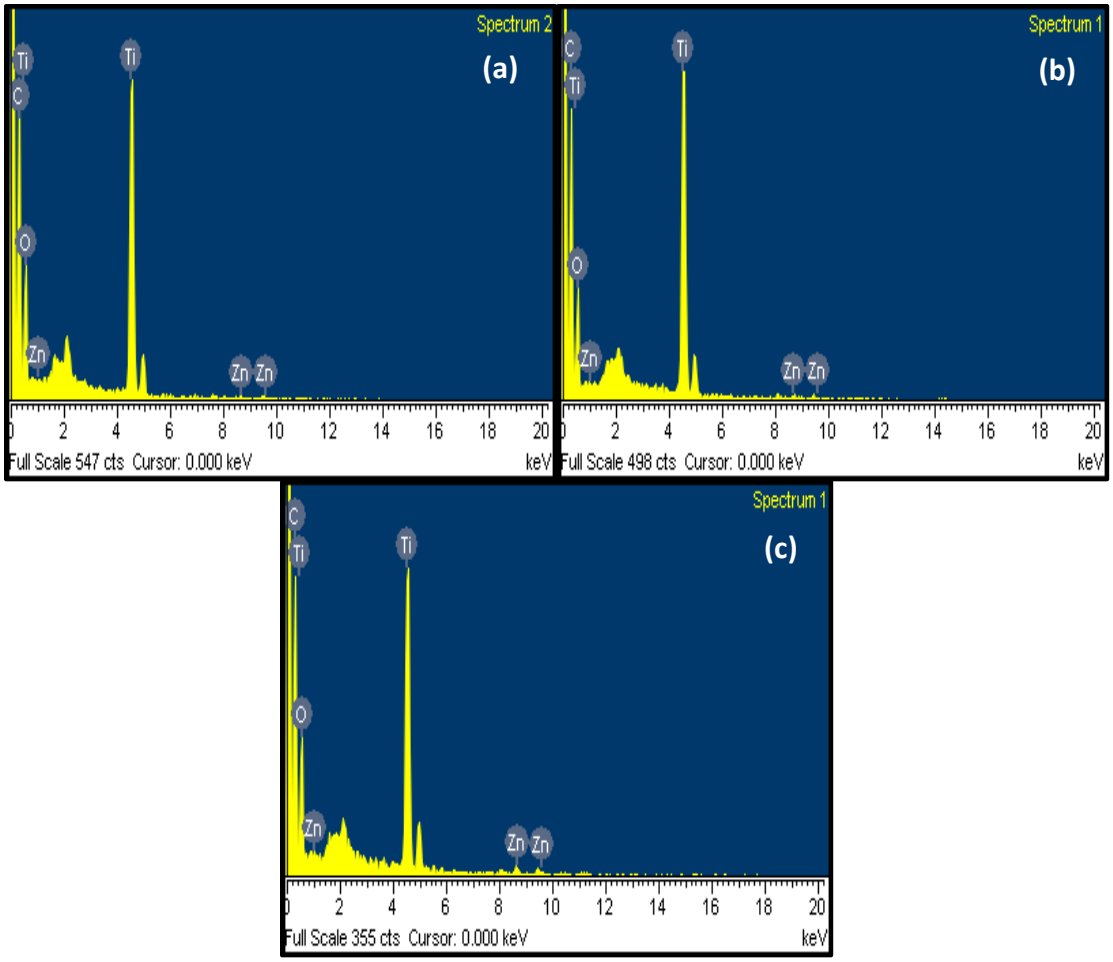

Figure 4.6 EDS analysis: (a) 0.5:1 GO-T (b) 1:1 GO-T (c) 2:1 GO-T

Table 4.4 EDS results of: (a) 0.5:1 GO-T (b) 1:1 GO-T (c) 2:1 GO-T

Element	Weight%	Atomic%
C K	36.88	51.79
O K	37.11	39.12
Ti K	25.26	8.90
Zn K	0.76	0.20
Totals	100.00	**(a)**

Element	Weight%	Atomic%
C K	37.55	53.37
O K	34.44	36.75
Ti K	26.93	9.60
Zn K	1.07	0.28
Totals	100.00	**(b)**

Element	Weight%	Atomic%
C K	38.89	53.05
O K	36.59	38.74
Ti K	22.83	7.13
Zn K	1.69	1.08
Totals	100.00	**(c)**

Moving towards the results of nanocomposites, EDS analysis in **figure 4.6** displays the existence of Ti, O, Zn and C content in each prepared sample. The prepared samples contained 2% Zn/N co-doped TiO_2 and GO with various ratios of GO (0.5, 1 and 2) and constant amount of catalyst. This can be clearly seen in the figure as carbon content is increasing with increase in the ratio of GO. This illustrates the correct composite formation. For the conformation of these results and the increase in carbon content, the results in **table 4.4** easily show the evidence.

4.2 Degradation studies

To check the optical properties of synthesized nanocatalysts and nanocomposites, degradation studies were done with methyl orange. In this study, a stock solution of 1000 ppm for methyl orange was prepared, from which a more dilute 10 ppm solution was obtained on which degradation studies were carried out for all the prepared samples.

First the study of all the prepared catalysts was done and the catalyst showing the best efficiency was then combined with GO to achieve extra efficiency. For catalysts study, solution of 50 mg of each catalyst and 10 ppm of methyl orange was prepared independently in 50 ml volumetric flasks and was kept in dark for 2 hours to attain adsorption-desorption equilibrium. Samples were then put in the photochemical reactor chamber under 300 W Xenon lamp and with constant stirring. 5 ml of every solution was

taken out after varying intervals. They were then centrifuged for 3 minutes at 10000 rpm to let the catalyst settle down. The solution other than the catalyst was observed from a UV-Visible spectrophotometer to study the photocatalytic activity and the level of degradation. MO have characteristic peak at 464 nm and decrease in the absorbance at this point specifies MO degradation.

It was witnessed from the degradation studies that all doped samples demonstrate more degradation than un-doped or pure TiO_2. When doped samples were compared with each other, 2% Zn/N co-doped TiO_2 showed best photocatalytic activity.

In **figure 4.9**, all the degradation spectra are shown for each prepared catalyst and the best results can be seen for the 2% Zn/N co-doped TiO_2 photocatalyst as the degradation rate is very high for that catalyst. The best sample showed degradation in 24 hours up to 80% which was only 60% in the case of pure TiO_2.

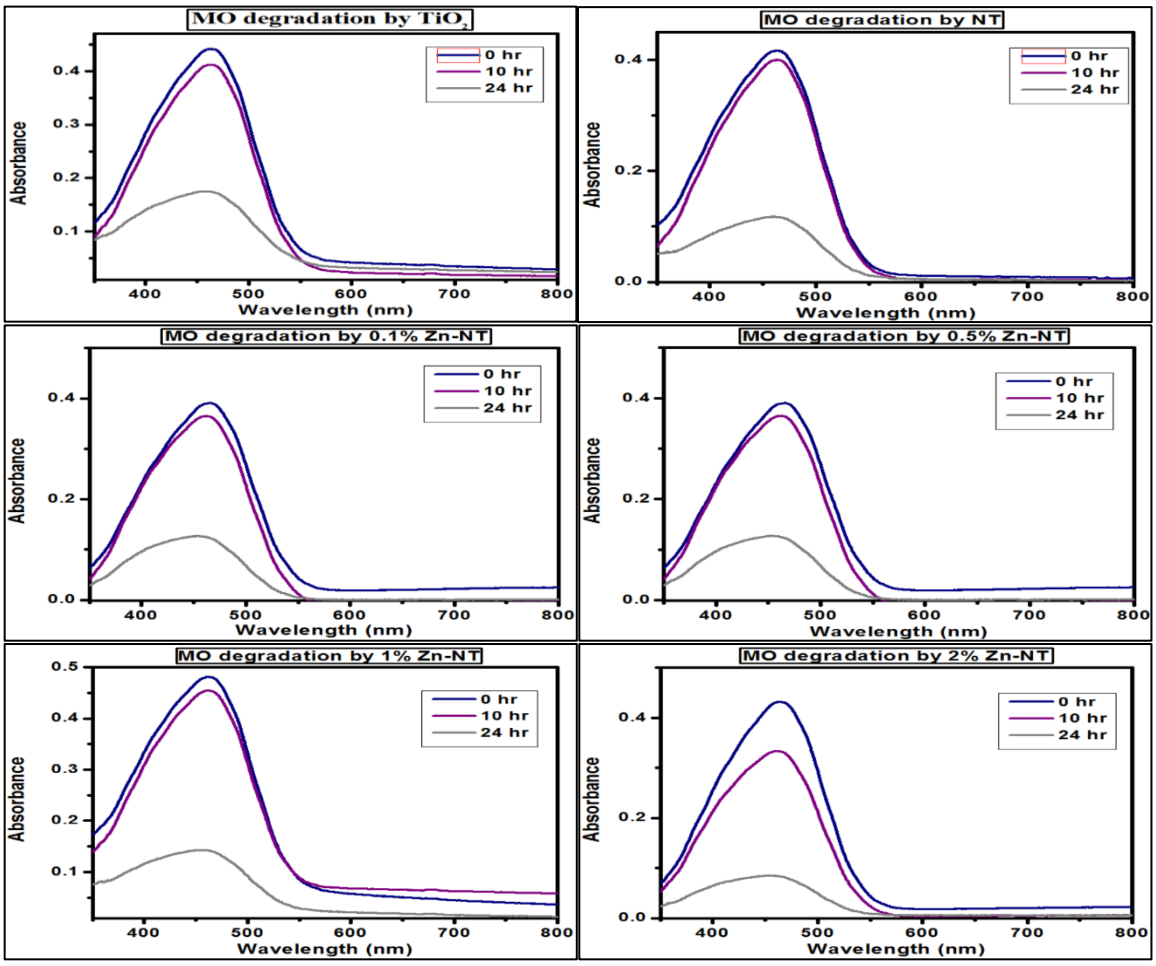

Figure 4.9 Degradation spectra of methyl orange using all prepared photocatalysts

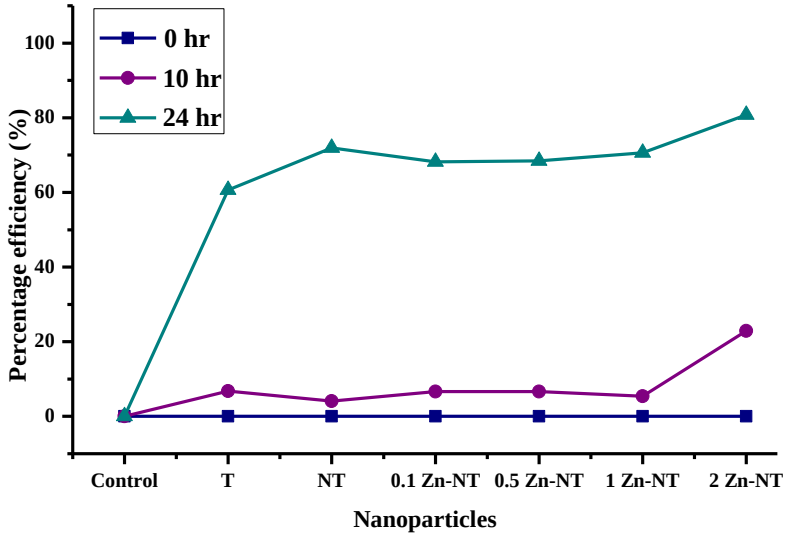

Figure 4.10 Efficiency of all prepared nanoparticles against degradation of MO

Figure 4.10 shows the efficiency of all the manufactured catalysts against MO degradation in percentage. It can be seen that 2% Zn/N co-doped TiO_2 shows greatest percentage efficiency than all the other catalysts.

It was evident from all the results that 2% Zn/N co-doped TiO_2 nanoparticles showed better efficiency of 80% in terms of degradation of MO than all other catalysts.

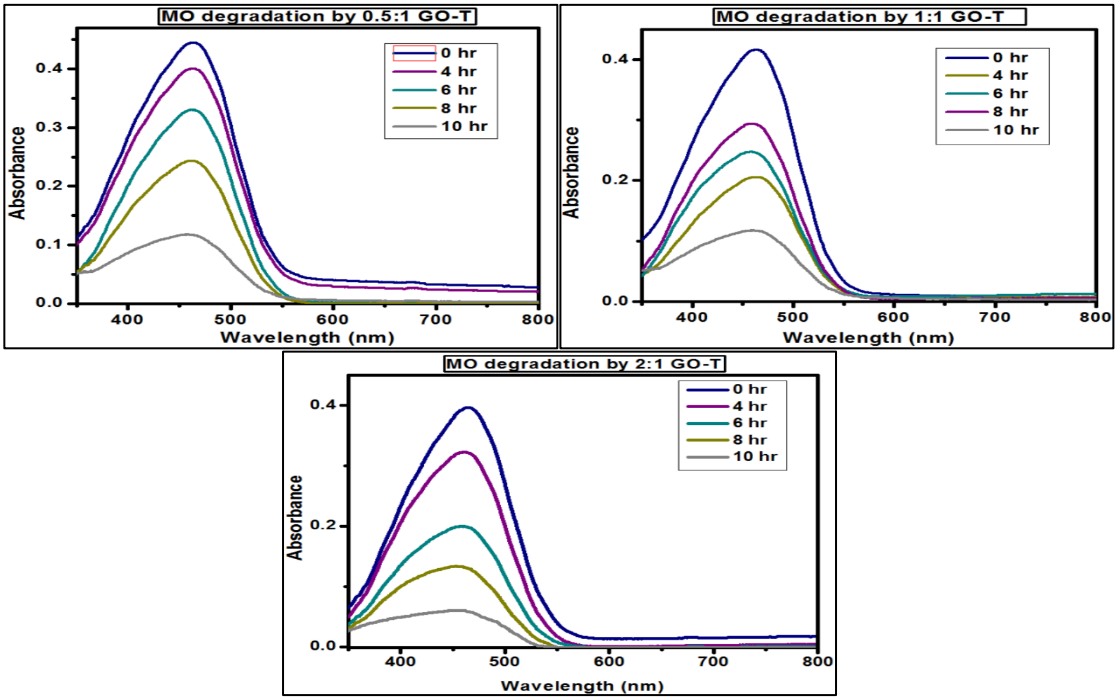

Figure 4.11 Degradation spectra of methyl orange using all prepared nanocomposites

The next step was to produce the nanocomposites based on GO and the best efficient catalyst with varying ratios of GO (0.5, 1, 2) and study their degradation rates on MO

similarly. Same method was taken, 50 mg of the prepared composites was taken separately with 0.01 mM of MO in a 50 ml volumetric flask and the solution was set aside in dark for 2 hours to reach adsorption-desorption equilibrium. This solution from dark was then removed and placed under visible light in a photocatalytic chamber. As the reaction rate was fast, 5 ml of solution was extracted from each solution at varying intervals. They were then centrifuged for 3 min at 10000 rpm and UV-Vis spectrophotometer was again used to study degradation rate. All spectra in **figure 4.11** show the degradation of methyl orange when nanocomposites were used. It can be seen that the highest concentration of GO based composite shows the highest efficiency against MO degradation. The overall degradation was done in 10 hrs total.

Moreover, this degradation rate is also compared for each composite in the manner of percentage efficiency and is shown in **figure 4.12**. The highest obtained efficiency is for 2:1 GO-T which is 85%.

The formula for percentage efficiency is:

Percentage Efficiency = $\{(A_O - A_t)/ A_O\}$ x 100

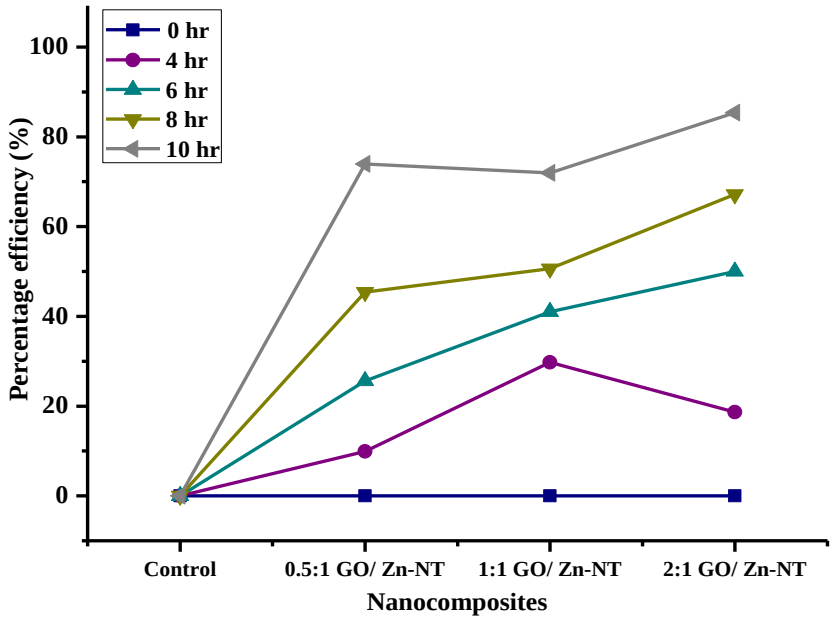

Figure 4.12 Efficiency of all prepared nanocomposites against degradation of MO

After all the calculated results and graphs obtained by the studies, it was confirmed that 2% Zn/N co-doped TiO_2 is proven as top catalyst and best nanocomposite is proven to be 2:1 GO- 2% Zn/N co-doped TiO_2 for the degradation of methyl orange.

5 CONCLUSION

Utilizing easy Sol-gel technique, zinc and nitrogen co-doped TiO_2 nanoparticles were synthesized. Zinc concentrations ranged from 0.1% to 2% where nitrogen concentration remained constant. To verify their optical and morphological characteristics, samples were characterized using XRD, SEM, EDS and UV-Vis spectroscopy. Crystallite size was found to be between 19.6-5.4 nm using XRD data interpretation and SEM data gave the particle size between 32-8.8 nm. TiO_2 showed maximum particle size and crystallite size while minimum particle and crystallite size was observed for 2% Zn/N co-doped TiO_2 having highest doping level of zinc. SEM images showed increase in agglomeration with increase in zinc doping levels. Methyl orange was used for degradation studies and the best activity was shown by 2% Zn/N co-doped TiO_2 nanoparticles with efficiency up to 80%. To further improve its properties, GO was combined with the best doped catalyst. For GO-T composites, degradation studies were again performed against methyl orange to check their efficiency. The efficiency increased to 85% for 2:1 GO-T which had the highest concentration of GO based composite.

Henceforward, all of these synthesized catalysts can be utilized for degradation studies of numerous additional organophosphates, pesticides and dyes and their competence can be determined.

6 REFERENCES

[1] Robinson, T., McMullan, G., Marchant, R., & Nigam, P. (2001). Remediation of dyes in textile effluent: a critical review on current treatment technologies with a proposed alternative. *Bioresource technology*, *77*(3), 247-255.

[2] Kulkarni, S. V., Blackwell, C. D., Blackard, A. L., Stackhouse, C. W., & Alexander, M. W. (1985). *Textile dyes and dyeing equipment: classification, properties and environmental aspects*. US Government Printing Office.

[3] McMullan, G., Meehan, C., Conneely, A., Kirby, N., Robinson, T., Nigam, P., ... & Smyth, W. F. (2001). Microbial decolourisation and degradation of textile dyes. *Applied microbiology and biotechnology*, *56*(1-2), 81-87.

[4] Han, F., Kambala, V. S. R., Srinivasan, M., Rajarathnam, D., & Naidu, R. (2009). Tailored titanium dioxide photocatalysts for the degradation of organic dyes in wastewater treatment: a review. Applied Catalysis A: General, 359(1-2), 25-40.

[5] Chakrabarti, S., & Dutta, B. K. (2004). Photocatalytic degradation of model textile dyes in wastewater using ZnO as semiconductor catalyst. *Journal of hazardous materials*, *112*(3), 269-278.

[6] Maira, A. J., Yeung, K. L., Lee, C. Y., Yue, P. L., & Chan, C. K. (2000). Size effects in gas-phase photo-oxidation of trichloroethylene using nanometer-sized TiO_2 catalysts. *Journal of Catalysis*, *192*(1), 185-196.

[7] Pascual, J., Camassel, J., & Mathieu, H. (1977). Resolved Quadrupolar Transition in TiO_2. *Physical Review Letters*, *39*(23), 1490.

[8] Wold, A. (1993). Photocatalytic properties of titanium dioxide (TiO_2). *Chemistry of Materials*, *5*(3), 280-283.

[9] Banerjee, S., Pillai, S. C., Falaras, P., O'shea, K. E., Byrne, J. A., & Dionysiou, D. D. (2014). New insights into the mechanism of visible light photocatalysis. *The journal of physical chemistry letters*, *5*(15), 2543-2554.

[10] Kumar, S. G., & Devi, L. G. (2011). Review on modified TiO_2 photocatalysis under UV/visible light: selected results and related mechanisms on interfacial charge carrier transfer dynamics. *The Journal of physical chemistry A*, *115*(46), 13211-13241.

[11] Zaleska, A. (2008). Doped-TiO2: a review. *Recent patents on engineering*, *2*(3), 157-164.

[12] Hoffmann, M. R., Martin, S. T., Choi, W., & Bahnemann, D. W. (1995). Environmental applications of semiconductor photocatalysis. *Chemical reviews*, *95*(1), 69-96.

[13]Rauf, M. A., Meetani, M. A., & Hisaindee, S. (2011). An overview on the photocatalytic degradation of azo dyes in the presence of TiO_2 doped with selective transition metals. *Desalination*, *276*(1-3), 13-27.

[14] Yang, L., Zhang, Y., Ruan, W., Zhao, B., Xu, W., & Lombardi, J. R. (2010). Improved surface-enhanced Raman scattering properties of TiO_2 nanoparticles by Zn dopant. *Journal of Raman Spectroscopy*, *41*(7), 721-726.

[15] Izumi, Y., Itoi, T., Peng, S., Oka, K., & Shibata, Y. (2009). Site structure and photocatalytic role of sulfur or nitrogen-doped titanium oxide with uniform mesopores under visible light. *The Journal of Physical Chemistry C*, *113*(16), 6706-6718.

[16] Sakthivel, S., Janczarek, M., & Kisch, H. (2004). Visible light activity and photoelectrochemical properties of nitrogen-doped TiO_2. *The Journal of Physical Chemistry B*, *108*(50), 19384-19387.

[17] Avilés-García, O., Espino-Valencia, J., Romero-Romero, R., Rico-Cerda, J., Arroyo-Albiter, M., Solís-Casados, D., & Natividad-Rangel, R. (2018). Enhanced photocatalytic activity of Titania by co-doping with Mo and W. *Catalysts*, *8*(12), 631.

[18] Štengl, V., Bakardjieva, S., Grygar, T. M., Bludská, J., & Kormunda, M. (2013). TiO_2-graphene oxide nanocomposite as advanced photocatalytic materials. *Chemistry Central Journal*, *7*(1), 41.

[19] Martins, P. M., Ferreira, C. G., Silva, A. R., Magalhães, B., Alves, M. M., Pereira, L., ... & Lanceros-Méndez, S. (2018). TiO_2/graphene and TiO_2/graphene oxide nanocomposites for photocatalytic applications: A computer modeling and experimental study. *Composites Part B: Engineering*, *145*, 39-46.

[20] Malekshahi Byranvand, M., Nemati Kharat, A., Fatholahi, L., & Malekshahi Beiranvand, Z. (2013). A review on synthesis of nano-TiO_2 via different methods. *Journal of nanostructures*, *3*(1), 1-9.

[21] Sajjadi, S. P. (2005). Sol-gel process and its application in nanotechnology. *Journal of Polymer Engineering and Technology*, *13*, 38-41.

[22] Ullattil, S. G., & Periyat, P. (2017). Sol-gel synthesis of titanium dioxide. In *Sol-Gel Materials for Energy, Environment and Electronic Applications* (pp. 271-283). Springer, Cham.

[23] Kumar, A., Yadav, N., Bhatt, M., Mishra, N. K., Chaudhary, P., & Singh, R. (2015). Sol-gel derived nanomaterials and its applications: a review. *Research Journal of Chemical Sciences* _____ *ISSN*, *2231*, 606X.

[24] Zhu, Y., Murali, S., Cai, W., Li, X., Suk, J. W., Potts, J. R., & Ruoff, R. S. (2010). Graphene and graphene oxide: synthesis, properties, and applications. *Advanced materials*, *22*(35), 3906-3924.

[25] Paulchamy, B., Arthi, G., & Lignesh, B. D. (2015). A simple approach to stepwise synthesis of graphene oxide nanomaterial. *Journal of Nano medicine & Nanotechnology*, *6*(1), 1.

[26] Mai, Y. J., Wang, X. L., Xiang, J. Y., Qiao, Y. Q., Zhang, D., Gu, C. D., & Tu, J. P. (2011). CuO/graphene composite as anode materials for lithium-ion batteries. *Electrochimica Acta*, *56*(5), 2306-2311.

[27] Li, B., & Cao, H. (2011). ZnO@ graphene composite with enhanced performance for the removal of dye from water. *Journal of Materials Chemistry*, *21*(10), 3346-3349.

[28] Zhang, M., Lei, D., Du, Z., Yin, X., Chen, L., Li, Q., Wang, T. (2011). Fast synthesis of SnO_2/graphene composites by reducing graphene oxide with stannous ions. *Journal of Materials Chemistry*, *21*(6), 1673-1676.

[29] Xu, X. R., Li, H. B., Wang, W. H., & Gu, J. D. (2004). Degradation of dyes in aqueous solutions by the Fenton process. *Chemosphere*, *57*(7), 595-600.

[30] Konstantinou, I. K., & Albanis, T. A. (2004). TiO_2-assisted photocatalytic degradation of azo dyes in aqueous solution: kinetic and mechanistic investigations: a review. *Applied Catalysis B: Environmental*, *49*(1), 1-14.

[31] Sandberg, R. G., Henderson, G. H., White, R. D., & Eyring, E. M. (1972). Kinetics of acid dissociation-ion recombination of aqueous methyl orange. *The Journal of Physical Chemistry*, *76*(26), 4023-4025.

[32] Ajmal, A., Majeed, I., Malik, R. N., Idriss, H., & Nadeem, M. A. (2014). Principles and mechanisms of photocatalytic dye degradation on TiO_2 based photocatalysts: a comparative overview. *Rsc Advances*, *4*(70), 37003-37026.

[33] Fujishima, A., & Honda, K. (1972). Electrochemical photolysis of water at a semiconductor electrode. *Nature*, *238*(5358), 37-38.

[34] Han, H., & Bai, R. (2009). Buoyant photocatalyst with greatly enhanced visible-light activity prepared through a low temperature hydrothermal method. *Industrial & Engineering Chemistry Research*, *48*(6), 2891-2898.

[35] Frank, S. N., & Bard, A. J. (1977). Heterogeneous photocatalytic oxidation of cyanide ion in aqueous solutions at titanium dioxide powder. *Journal of the American Chemical Society*, *99*(1), 303-304.

[36] Wang, C. C., & Ying, J. Y. (1999). Sol− gel synthesis and hydrothermal processing of anatase and rutile Titania nanocrystals. *Chemistry of Materials*, *11*(11), 3113-3120.

[37] Yang, H., Zhang, K., Shi, R., Li, X., Dong, X., & Yu, Y. (2006). Sol–gel synthesis of TiO_2 nanoparticles and photocatalytic degradation of methyl orange in aqueous TiO_2 suspensions. *Journal of Alloys and Compounds*, *413*(1), 302-306.

[38] Hamadanian, M., Reisi-Vanani, A., & Majedi, A. (2010). Sol-gel preparation and characterization of Co/TiO_2 nanoparticles: application to the degradation of methyl orange. *Journal of the Iranian Chemical Society*, *7*(1), S52-S58.

[39] Vijayalakshmi, R., & Rajendran, V. (2012). Synthesis and characterization of nano-TiO_2 via different methods. *Arch App Sci Res*, *4*(2), 1183-1190.

[40] Sharma, A., Karn, R. K., & Pandiyan, S. K. (2014). Synthesis of TiO_2 Nanoparticles by Sol-gel Method and Their Characterization. *J. Basic Appl. Eng. Res.*, *1*, 1-5.

[41] Sabry, R. S., Al-Haidarie, Y. K., & Kudhier, M. A. (2016). Synthesis and photocatalytic activity of TiO_2 nanoparticles prepared by sol–gel method. *Journal of Sol-Gel Science and Technology*, *78*(2), 299-306.

[42] Sathish, M., Viswanathan, B., Viswanath, R. P., & Gopinath, C. S. (2005). Synthesis, characterization, electronic structure, and photocatalytic activity of nitrogen-doped TiO_2 nanocatalyst. *Chemistry of materials*, *17*(25), 6349-6353.

[43] Huang, Y. U., Zheng, X., Zhongyi, Y. I. N., Feng, T. A. G., Beibei, F. A. N. G., & Keshan, H. O. U. (2007). Preparation of Nitrogen-doped TiO_2 Nanoparticle Catalyst and Its Catalytic Activity under Visible Light** Supported by the Science and Technology Research Program of Chongqing Education Commission (KJ050702), and the Natural Science Foundation Project of Chongqing Science and Technology Commission (No. 2007BB7208). *Chinese Journal of Chemical Engineering*, *15*(6), 802-807.

[44] Senthilnathan, J., & Philip, L. (2010). Photocatalytic degradation of lindane under UV and visible light using N-doped TiO_2. *Chemical Engineering Journal*, *161*(1), 83-92.

[45] Hassanvand, A., Sohrabi, M., Royaee, S. J., & Jafarikajour, M. (2014). Preparation and characterization of nitrogen doped TiO_2 nanoparticles as an effective catalyst in photodegradation of phenol under visible light. In *Advanced Materials Research* (Vol. 875, pp. 28-33). Trans Tech Publications.

[46] Abdullah, A. M., Al-Thani, N. J., Tawbi, K., & Al-Kandari, H. (2016). Carbon/nitrogen-doped TiO_2: new synthesis route, characterization and application for phenol degradation. *Arabian Journal of Chemistry*, *9*(2), 229-237.

[47] Zhang, H., Liang, Y., Wu, X., & Zheng, H. (2012). Enhanced photocatalytic activity of (Zn, N)-codoped TiO_2 nanoparticles. *Materials Research Bulletin*, *47*(9), 2188-2192.

[48] Aware, D. V., & Jadhav, S. S. (2016). Synthesis, characterization and photocatalytic applications of Zn-doped TiO_2 nanoparticles by sol–gel method. *Applied Nanoscience*, *6*(7), 965-972.

[49]Rimoldi, L., Pargoletti, E., Meroni, D., Falletta, E., Cerrato, G., Turco, F., & Cappelletti, G. (2018). Concurrent role of metal (Sn, Zn) and N species in enhancing the photocatalytic activity of TiO_2 under solar light. *Catalysis Today*, *313*, 40-46.

[50] Wattanawikkam, C., & Pecharapa, W. (2015). Synthesis and characterization of Zn-doped TiO_2 nanoparticles via sonochemical method. *Integrated Ferroelectrics*, *165*(1), 167-175.

[51]Yu, Y., Wang, J., Li, W., Zheng, W., & Cao, Y. (2015). Doping mechanism of Zn^{2+} ions in Zn-doped TiO_2 prepared by a sol–gel method. *CrystEngComm*, *17*(27), 5074-5080.

[52] Krishnamoorthy, K., Mohan, R., & Kim, S. J. (2011). Graphene oxide as a photocatalytic material. *Applied Physics Letters*, *98*(24), 244101.

[53] Hummers Jr, W. S., & Offeman, R. E. (1958). Preparation of graphitic oxide. *Journal of the American Chemical Society*, *80*(6), 1339-1339.

[54] Chen, J., Yao, B., Li, C., & Shi, G. (2013). An improved Hummers method for eco-friendly synthesis of graphene oxide. *Carbon*, *64*, 225-229.

[55] Shahriary, L., & Athawale, A. A. (2014). Graphene oxide synthesized by using modified hummers approach. *Int. J. Renew. Energy Environ. Eng*, *2*(01), 58-63.

[56] Paulchamy, B., Arthi, G., & Lignesh, B. D. (2015). A simple approach to stepwise synthesis of graphene oxide nanomaterial. *Journal of Nanomedicine & Nanotechnology*, *6*(1), 1.

[57] Khalid, N. R., Ahmed, E., Hong, Z., Zhang, Y., & Ahmad, M. (2012). Nitrogen doped TiO_2 nanoparticles decorated on graphene sheets for photocatalysis applications. *Current Applied Physics*, *12*(6), 1485-1492.

[58] Khalid, N. R., Ahmed, E., Hong, Z., Ahmad, M., Zhang, Y., &Khalid, S. (2013). Cu-doped TiO_2 nanoparticles/graphene composites for efficient visible-light photocatalysis. *Ceramics International*, *39*(6), 7107-7113.

[59] Shang, X., Zhang, M., Wang, X., & Yang, Y. (2014). Sulfur, nitrogen-doped TiO_2/graphene oxide composites as a high performance photocatalyst. *Journal of Experimental Nanoscience*, *9*(7), 749-761.

[60] Yadav, H. M., & Kim, J. S. (2016). Solvothermal synthesis of anatase TiO_2-graphene oxide nanocomposites and their photocatalytic performance. *Journal of Alloys and Compounds*, *688*, 123-129.